The Stratigraphic Record of Minibasin Subsidence

Christopher A-L. Jackson[1]*[∞]
Oliver B. Duffy[1]
Naiara Fernandez[1]
Tim P. Dooley[1]
Michael R. Hudec[1]
Martin P.A. Jackson[1]
George Burg[2]

[1]*Bureau of Economic Geology, Jackson School of Geoscience, University of Texas at Austin, University Station, Box X, Austin, Texas, 78713-8924, USA*

[2]*Condor Petroleum Inc, Suite 2400, 144-4th Ave SW, Calgary, AB, T2P 3N4, Canada*

**present address: Basins Research Group (BRG), Department of Earth Science and Engineering, Imperial College, Prince Consort Road, London, SW7 2BP, UK*

[∞]*corresponding author: c.jackson@imperial.ac.uk (C.A-L. Jackson)*

ABSTRACT

Minibasins are fundamental components of many salt-bearing sedimentary basins, where they may host large volumes of hydrocarbons. Although we understand the basic mechanics governing their subsidence, we know surprisingly little of how minibasins subside in three-dimensions over geological timescales, or what controls such variability. Such knowledge would improve our ability to constrain initial salt volumes in sedimentary basins, the timing of salt welding, and the distribution and likely charging histories of suprasalt hydrocarbon reservoirs. We use 3D seismic reflection data from the Precaspian Basin, onshore Kazakhstan to reveal the subsidence histories of 16, Upper Permian-to-Triassic, suprasalt minibasins. These minibasins subsided into a Lower-to-Middle Permian salt layer that contained numerous relatively strong, clastic-dominated minibasins encased during an earlier, latest Permian phase of diapirism; because of this, the salt varied in thickness. Suprasalt minibasins contain a stratigraphic record of symmetric (bowl-shaped units) and then asymmetric (wedge-shaped units) subsidence, with this change in style seemingly occurring at different times in different minibasins, and most likely prior to welding. We use our observations from the Precaspian Basin and physical models to explore the potential controls on temporal and

spatial variations in minibasin subsidence, before assessing which of these might be applicable to our natural example. We conclude that due to uncertainties in the original spatial relationships between encased and suprasalt minibasins, and the timing of changes in style of subsidence between individual minibasins, it is unclear why such complex temporal and spatial variations in subsidence occur in the Precaspian Basin. Regardless of what controls the observed variability, we argue that vertical changes in minibasin stratigraphic architecture may not record the initial (depositional) thickness of underlying salt or the timing of salt welding; this latter point is critical when attempting to constrain the timing of potential hydraulic communication between sub-salt source rocks and suprasalt reservoirs. Furthermore, temporal changes in minibasin subsidence style will likely control suprasalt reservoir distribution and trapping style.

INTRODUCTION

A minibasin is defined as a "synkinematic basin subsiding into relatively thick autochthonous or allochthonous salt" (Jackson and Talbot, 1991, p.16; Fig. 1). Minibasins are fundamental components of many salt-bearing sedimentary basins and are remarkable in that, despite their relatively small size (typically a few kilometres to tens of kilometres in diameter; Fig. 1B, C and E), they can subside faster (>1-10 km/Myr) than basins formed on continental or oceanic crust (e.g. Worrall and Snelson, 1989; Prather, 2000). Due to their rapid subsidence rates and widespread development in some of the world's largest salt basins (e.g. Gulf of Mexico, Precaspian Basin, circum-South Atlantic; Hudec and Jackson, 2007), minibasins act as repositories for vast quantities of continent-derived sediment. Significant volumes of hydrocarbons may also be contained within minibasins, with their style of subsidence controlling the distribution of reservoir rocks and trap style (Fig. 1D) (e.g. Prather, 2000; Kane et al., 2012). More generally, minibasin stratigraphic architecture may record the processes controlling basin subsidence and, more fundamentally, the thickness of underlying salt and the timing of salt welding (Fig. 1A) (Rowan and Weimer, 1998). Constraining past and present salt thicknesses (and hence, volumes) is a key challenge when attempting to unravel the geodynamics of continental breakup (e.g. Davison et al., 2012), whereas the timing of salt welding is of critical importance for understanding the potential for and the timing of the transmission of hydrocarbons through welds from subsalt source rocks into suprasalt reservoirs (Rowan, 2004).

Despite their ubiquity and importance, and although they are typically well-imaged in seismic reflection data and penetrated by numerous boreholes, surprisingly little is known about the variability of minibasin subsidence, and what controls this in time and space (see Clark et al. 1998 for an exception; Fig. 1E). This reflects how few published studies have employed high-quality, regionally-extensive 3D seismic reflection datasets to map their synkinematic strata, the architecture of which preserve a record of salt tectonic-related changes in accommodation. Using 2D seismic reflection and borehole data from the northern Gulf of Mexico, Rowan and Weimer (1998) document four types of

seismic-stratigraphic packages within Pliocene-Pleistocene minibasins subsiding into thick allochthonous salt. Each type defines a different style of minibasin subsidence, with periods of broadly symmetrical subsidence recorded by 'bowls' and 'layers', and asymmetric subsidence and minibasin tilting defined by 'wedges' (Fig. 1A and C). Rowan and Weimer (1998) conclude the transition from bowl- to wedge-shaped packages is driven by and thus records minibasin welding (see Fig. 1A). In contrast, Hudec et al. (2009), also using 2D seismic reflection data, show that variations in minibasin stratigraphic architecture may not simply document welding; rather, they infer offset stacking of bowl-shaped packages document: (i) minibasin genesis and subsequent subsidence under the influence of sedimentary topographic loading (see also Ge et al., 1997 and Jackson et al., 2015); (ii) syn-subsidence regional shortening; and/or (iii) horizontal translation of a minibasin array within a spreading canopy (e.g. Fig. 1D). Given that salt flow can be very three-dimensional, even in cases defined by simple minibasin downbuilding and passive diapirism, it is unlikely that two-dimensional profiles capture the true temporal and spatial complexity of minibasin subsidence (see Fig. 1E and F).

In this paper we consider the following three questions: (i) what are the key styles of stratigraphic architectures developed in minibasins?; (ii) what controls minibasin subsidence patterns?; and (iii) how do variations in minibasin subsidence impact hydrocarbon exploration in salt-bearing sedimentary basins? To answer these questions, we use high-quality 3D seismic reflection and borehole data to constrain subsidence patterns in 16 minibasins in the eastern Precaspian Basin, onshore Kazakhstan. The Precaspian Basin is an ideal place to conduct this study because: (i) the minibasins contain a thick (up to 5.5 km) stratigraphic fill documenting periods of distinct subsidence style during simple downbuilding and passive diapirism; (ii) the minibasins are shallowly buried (<1 km) beneath a structurally and stratigraphically simple cover and, as a result, are well-imaged in seismic reflection data; (iii) borehole data constrain the composition of underlying salt, indicating this contains a series of clastic-dominated, largely encased minibasins (Duffy et al., 2017; Fernandez et al., 2017). We show that subsidence patterns within and between adjacent minibasins can be complex, with an initial phase of symmetric subsidence (recorded by deposition of bowl-shaped units typically followed by a phase of asymmetric subsidence recorded by deposition of wedge-shaped units). This change in subsidence style likely occurred at different times in different minibasins, and, critically, *prior* to minibasin welding to presalt strata. Based on the regional geological setting of the Precaspian Basin and the results of physical models, we explore a range of mechanisms that could drive the observed subsidence patterns. We conclude by discussing the implications of our study for hydrocarbon exploration in salt-bearing sedimentary basins.

TECTONO-STRATIGRAPHIC FRAMEWORK

The study area is located in the southeastern Precaspian Basin, onshore Kazakhstan (Fig. 2). In the Early Devonian, the Precaspian Basin was part of a SE-dipping passive margin facing the Ural Ocean

(Barde et al., 2002a,b; Volozh et al., 2003). Subsequent Middle Devonian rifting was followed by Carboniferous post-rift thermal subsidence. By the middle Carboniferous, collision of the Eastern European and Kazakh plates resulted in the Ural Orogeny, causing uplift of the Precaspian Basin's eastern flank (Brunet et al., 1999; Barde et al., 2002b). By the end of the Early Permian, the Precaspian Basin was represented by a rapidly subsiding foreland basin located in the Uralian foreland. During this time, the basin became isolated from the Tethys Ocean, and a thick (up to 4.5 km in the basin; c. 2 km in the study area; Fig. 2A), Kungurian-to-Kazanian salt sequence was deposited, which passed laterally into clastic and carbonate rocks at the basin margins (Fig. 3) (Gralla and Marsky, 2000; Barde et al., 2002b, Volozh et al., 2003). During the Late Permian, clastic detritus was shed off the rising Ural Mountains, loading the salt and expelling it basinward towards the west. Salt flow resulted in the formation of broadly N-trending salt walls and related expulsion rollovers, both of which were orientated sub-parallel to the local basin margin (Fig. 2B). Farther west, within our study area, salt walls display an overall polygonal arrangement; individual walls are up to 20 km long, 8 km wide, have a vertical relief of up to 5.5 km (Figs 2, 4A and 5), and bound sub-circular minibasins (Duffy et al., 2017; Fernandez et al., 2017).

Relatively little has been published on the detailed salt-tectonic history of the Precaspian Basin (e.g. Sokolova et al., 1973; Gralla and Marsky, 2000; González Muñoz et al., 2001; Barde et al., 2002a,b; Volozh et al., 2003a,b; Duffy et al., 2017; Fernandez et al., 2017). However, recent work by Duffy et al. (2017) and Fernandez et al. (2017) using data from onshore Kazakhstan show that, during the latest Permian, a series of minibasins subsided into the Lower-to-Middle Permian salt. These evaporite- and non-marine clastic-bearing minibasins (see Barde et al. 2002b) are now fully or partly encased in and lie in the lower half of the salt, and are typically welded to presalt strata (Figs 4 and 5). They are sub-circular to ovate in plan-view and up to 3000 m thick, with the thinnest encased minibasins (<1000 meters thick) clustering near and commonly being in direct contact with suprasalt minibasins (see below) across 'tertiary' welds (Fig. 5) (*sensu* Jackson and Cramez, 1989). Thicker encased minibasins are typically located in the centres of the salt diapirs and are welded to suprasalt minibasins (Fig. 5). Minibasin encasement most likely occurred due to canopy emplacement driven by salt expulsion from beneath adjacent, more rapidly subsiding minibasins, although other mechanisms are possible (see Fig. 3 in Fernandez et al., 2017). Regardless of their origin, the presence of encased minibasins means the salt varied in thickness during subsidence of the suprasalt minibasins, being relatively thin above encased basins, and thick within intervening diapiric feeders that fed the canopy (Fig. 5).

Another generation of minibasins formed in the latest Permian to Triassic. These suprasalt minibasins are up to 10 km in diameter and 5.5 km deep, and are welded to presalt strata or encased minibasins (see above) (Figs 4 and 5) (see also Duffy et al., 2017). A top Permian unconformity, which cannot be identified in seismic reflection data, is preserved within the suprasalt minibasins; this may record regional shortening related to the protracted, polyphase, Uralian Orogeny (Fig. 3)

(Sokolova et al., 1973; Barde et al., 2002a; Volozh et al., 2003). The structural style, stratigraphic architecture, and subsidence history of these suprasalt minibasins form the focus of our study.

Triassic strata within the suprasalt minibasins are capped by the Base Jurassic Unconformity (BJU; Figs 3 and 5), a major erosional unconformity recording ca. 35 Myr of uplift and erosion associated with the Late Triassic Cimmerian orogeny (e.g. Volozh et al., 2003a; Ismail-Zadeh et al., 2008). This major tectonic event uplifted the Precaspian Basin, resulting in erosion of the crests of salt diapirs and the upper parts of adjacent suprasalt minibasins (Figs 3 and 5). A relatively thin (<1 km), broadly tabular, Jurassic-to-Lower Cretaceous succession caps the diapirs and flanking minibasins (Figs 2 and 5). Regional shortening in the Late Cretaceous and Oligo-Miocene, driven by the collision of Arabia and India with Asia, squeezed and rejuvenated diapirs between laterally mobile suprasalt minibasins (Volozh et al., 2003a; Duffy et al., 2017; Fernandez et al., 2017). As discussed by Duffy et al. (2017), where encased minibasins were absent, the suprasalt minibasins were able to weld, whereas where encased minibasins were present, suprasalt minibasins were kept apart by the intervening encased minibasins. As a result, post-subsidence shortening means that some suprasalt minibasins are closer together than when they formed, and their spatial relationship to the encased minibasins has been modified.

DATASET AND METHODS

We use two time-migrated 3D seismic reflection datasets that together cover 2532 km^2 of the eastern Precaspian Basin, onshore Kazakhstan; these surveys have been merged to produce one interpretable volume. The 2010 (1252 km^2) and 2011 (1280 km^2) surveys both image to 6 seconds two-way time (s TWT) and have a vertical sample rate of 2 milliseconds (ms). Inline (E-W) and crossline (N-S) spacing is 20 m. The seismic data are presented with Society of Economic Geologists (SEG) 'normal polarity', where a downward increase in acoustic impedance is represented by a positive reflection event (white on seismic sections) and a downward decrease in acoustic impedance is represented by a negative reflection event (black on seismic sections). Our time-migrated dataset has better stratigraphic imaging of suprasalt minibasins than the depth-migrated volume used by Duffy et al. (2017) and Fernandez et al. (2017) in their analysis of the more deeply buried encased minibasins (Figs 4 and 5). We therefore use the time-migrated dataset for our detailed analysis of the suprasalt minibasins. However, because of their better imaging of deep structures, we here use two images from these depth-migrated seismic data; (i) a top-allochthonous-salt depth map (Fig. 4A); and (ii) a top-encased-minibasins depth map (Fig. 4B) (see Duffy et al., 2017 and Fernandez et al., 2017).

Numerous boreholes lie within the area covered by the seismic reflection dataset, although most are relatively shallow, terminating in Upper Triassic strata. The two boreholes penetrating older (i.e. Late Permian) strata contained in encased basins (KN-501 and KN-E-201-205) penetrate areas of thick salt and do not intersect intervening suprasalt basins; because of this, the age of the stratigraphy

within the suprasalt minibasins is thus poorly constrained (Fernandez et al., 2017). However, given the Kungurian to Kazanian (Permian) age of the salt, and the stratigraphic position of the base Jurassic Unconformity, the encased and suprasalt basins are likely Late Permian to Triassic (Figs 3 and 5). The lack of borehole data mean we utilize seismic-stratigraphic relationships to define genetic packages we believe document discrete phases of minibasin subsidence (see below).

EVIDENCE FOR COMPLEX MINIBASIN TILTING

Description

The salt structures (and their encased minibasins) flank 22 suprasalt minibasins that are up to 10 km in diameter and up to 5.5 km deep (i.e. between top salt and base Jurassic; Figs 4 and 5). Suprasalt minibasins are typically welded to presalt strata (primary welds) or, in several cases, against or atop encased minibasins (tertiary welds) (Fig. 5) (see also Duffy et al., 2017). Reflections within the suprasalt minibasins show highly variable dips (see below), but invariably onlap onto and are upturned against flanking diapirs (Fig. 5).

In the absence of boreholes directly constraining the age of the stratigraphic infill of suprasalt minibasins, we use reflection terminations (e.g. onlap, erosional truncations) to define geometrically distinct seismic sequences (e.g. bowls, wedges, layers; Fig. 1A-C). It should be noted however that, because of their unique subsidence and sedimentation histories, the number of reflections mapped within each minibasin varies, and it is not possible to confidently correlate seismic sequences between them. These issues notwithstanding, we identify and map a range of seismic-stratigraphic architectures that document the unique subsidence histories of individual minibasins. In the following sections we provide detailed descriptions of the seismic-stratigraphic architecture of three of the 22 minibasins (minibasins 7, 9 and 18; Figs 4C). These minibasins are very well-imaged, and capture the full range of seismic-stratigraphic architectures and subsidence patterns identified within the other 13 suprasalt minibasins.

Minibasin 9 – Vertical symmetrical subsidence superseded by unidirectional asymmetrical subsidence

Minibasin 9 is located in the north-central part of the seismic dataset (Fig. 4C). Minibasin 9 is not directly underlain by encased basins, although a relatively large encased minibasin lies c. 5 km to the south-southwest (labelled ‘U’ in Fig. 4C). We identify five seismic-stratigraphic packages in Minibasin 9, arranged into three units:

Unit 1. This is directly underlain by top allochthonous salt or its equivalent weld, and is up to 1400 ms (TWT) thick (true stratigraphic thickness). Unit 1 comprises several bowl-shaped packages (cf.

Fig. 1A) that thin towards and onlap onto flanking salt structures. Reflections within Unit 1 dip eastward (Fig. 6A and B).

Unit 2. This is up 200 ms (TWT) thick and comprises a series of wedge-shaped packages (cf. Fig. 1A) that display subtly different thickness patterns (Units 2A-C; Fig. 6A). The lowermost unit thickens east-northeastwards, pinching out west-southwestwards onto the upturned, east-dipping western margin of the underlying bowl-shaped package of Unit 1 (Unit 2A; Fig. 6A and C). In contrast, the middle package dips and thickens eastwards, thus its locus of deposition is offset (c. 1.6 km) slightly south-eastwards from that defined in 2A (Unit 2B; Fig. 6D). Finally, the depositional locus of the uppermost package is offset a further c. 2 km east-southeastwards of that defined in Unit 2B, being located immediately adjacent to the salt-sediment interface (Unit 2C; Fig. 6A and E).

Unit 3. This unit is up to 400 ms (TWT) thick and is composed of broadly tabular packages of reflections that are upturned above the steep-dipping flank of the diapir bounding the minibasins eastern margin, and which are erosionally-truncated at the present land surface. Note that due to post-depositional deformation and arching above the flanking diapirs, and associated erosional truncation of their upper surfaces, these tabular packages have a broadly wedge-shaped form (Fig. 6A). Basal reflections in Unit 3 are parallel to those in the upper part of Unit 3, the significance of which we discuss further below (Fig. 6A).

Minibasin 7 – Vertical subsidence superseded by bi-directional asymmetric subsidence

Minibasin 7 is located near the western margin of the seismic dataset, and is bound on its eastern and southern flanks by encased minibasins (labelled ‘V’ and ‘W’ in Figs 4C and 7A). We identify six seismic-stratigraphic packages in Minibasin 7, arranged into three units:

Unit 1. This directly overlies allochthonous salt or its equivalent weld, and is up to 830 ms (TWT) thick (true stratigraphic thickness) (Fig. 7A). Unit 1 comprises bowl-shaped packages that thin towards and onlap onto the flanking diapirs, with internal reflections presently dipping eastward (Fig. 7A and B).

Unit 2. This unit is up to 1000 ms (TWT) thick and comprises three wedge-shaped packages (Fig. 7A). A key observation we make is that, although geometrically similar, wedge-shaped packages in Unit 2 vary dramatically in their direction of thickening and present dip. The lowermost package, thickens north-westwards, despite its internal reflections presently dipping east-southeastwards (Unit 2A; Fig. 7C). In contrast, the overlying package thickens northward, with internal reflections dipping

east-southeastwards (Unit 2B; Fig. 7D), whereas the uppermost two packages thicken south-westwards, with internal reflections dipping south-eastwards (Units 2C and D; Fig. 7D and E).

Unit 3. This unit is up to 1250 ms (TWT) thick and is composed of broadly tabular packages of reflections. We define two sub-units in Unit 3; a lower sub-unit that dips south-eastwards and which is truncated below the base Jurassic unconformity towards the north-west (Unit 3A; Fig. 7A and F), and more gently-dipping upper sub-unit that overlies the unconformity and that also dips south-eastwards (Unit 3B; Fig. 7A).

Minibasin 18 – Vertical subsidence in adjoining basins superseded by asymmetric subsidence and abrupt shifts in depocentre

Minibasin 18 is located in the south-eastern part of the seismic dataset, where a cluster of three encased minibasins bound its south-western flank (labelled 'X', 'Y' and 'Z'; Figs 4C and 8A). We sub-divide Minibasin 18 into three main seismic-stratigraphic units:

Unit 1. This directly overlies allochthonous salt or presalt strata across a primary weld, and is up to 520 ms (TWT) thick (true stratigraphic thickness). Unit 1 is internally defined by two bowl-shaped packages that thin towards and onlap onto flanking diapirs, and which are partly separated by a low-relief, slightly NW-elongate diapir ('IMB' in Fig. 8A and B). Reflections within Unit 1 presently dip northwards (Fig. 8B).

Unit 2. This is up to 2000 ms (TWT) thick and comprises two main wedge-shaped packages. As we observed in minibasin 7, wedge-shaped packages in minibasin 18 display strikingly different thickness patterns despite being geometrically similar. The lowermost package thickens north-eastward, although internal reflections presently dip west-southwestwards (Unit 2A; Fig. 8A and C). In contrast, Unit 2B thickens northward, with internal reflections presently dipping west-southwestwards (Unit 2B; Fig. 8A and D).

Unit 3. This unit is up to 442 ms (TWT) thick and is composed of broadly tabular packages of reflections. As in minibasin 7, we define two sub-units in Unit 3; a lower sub-unit that dips gently south-southwestwards, which is truncated below the base Jurassic unconformity towards the north-northeast, and which is upturned against (in its lower part) and caps (in its upper part) the diapir forming the south-western margin of the minibasin (Unit 3A; Fig. 8A). Unit 3B overlies the base Jurassic Unconformity, is more gently dipping than 3A, and is truncated at the present land surface (Fig. 8A).

Interpretation

The lower parts of all three minibasins are composed of bowl-shaped packages (Unit 1). We follow Rowan and Weimer (1998) and interpret this seismic sequence architecture records an initial phase of relatively simple symmetric subsidence of the minibasins into underlying salt (see also Hudec et al., 2009; see Fig. 1A-C). In the case of minibasin 18, initial subsidence was characterized by the formation of two bowl-shaped minibasins separated by a small diapir; these two minibasins eventually coalesced by the end of Unit 1 to form a single minibasin (Fig. 8A and B).

The middle and upper parts of minibasins 7, 9 and 18 comprise wedge- (Unit 2) rather than bowl-shaped seismic sequences, thus recording a phase of asymmetrical subsidence and minibasin tilting (cf. Rowan and Weimer, 1998 and Hudec et al., 2009). However, shifts in the locus of maximum thickness of wedge-shaped packages within minibasins indicate their directions of tilting varied through time. In the case of minibasin 9, this subsidence variability was quite subtle, with broadly east-northeastward tilting (i.e. Unit 2A; Fig. 6C) being superseded by eastward tilting (Units 2B and C; Fig. 6D and E). In contrast, more extreme variability in tilting direction is documented in Minibasin 7, which initially tilted west-northwestwards (i.e. Unit 2A; Fig. 7C), then north-northwestward (Unit 2B; Fig. 7D), and eventually south-eastward (Units 2C and D; Fig. 7E).

All three minibasins are capped by tabular (Unit 3) sequences (Figs 6-8), which we interpret record: (i) sediment aggradation during uniform minibasin subsidence; or (ii) sediment aggradation above welded minibasins and flanking diapirs. We note Unit 3 is truncated by the base Jurassic Unconformity in all three minibasins, with tabular units below the unconformity being conformable with underlying, steeply dipping wedge-shaped sequences (i.e. Unit 3A), and those above being more gently-dipping and conformable with the unconformity (i.e. Unit 3B; see Figs 7A and 8A). We also note that internal reflections within the lower, pre-base Jurassic Unconformity parts of the tabular units (i.e. Unit 3A) have broadly the same dominant dip that characterising the deeper minibasin as a whole; this contrasts with the underlying, wedge-shaped packages, whose internal dips and thickening trends can be almost 180° to their present overall dip (Figs 7C and D, and 8C and D). Based on these observations we interpret Unit 3A records sediment aggradation after minibasin welding (cf. Fig. 1A). Pre-Jurassic regional shortening (Duffy et al., 2017) then caused diapir squeezing and minibasin tilting; as a result, wedge-shaped packages now thicken up-structure (i.e. Figs 7A and 8A), or dip in a different direction to that which characterized the subsidence regime at the time of their deposition. Uppermost minibasin strata were truncated along the base Jurassic Unconformity, which was ultimately being capped by tabular packages deposited during regional basin subsidence (Unit 3B; Figs 5-8). Subsequent, Early Cretaceous regional shortening then caused further diapir squeezing and arching of their tabular roofs (Figs 5-8) (Duffy et al., 2017).

ARRAY-SCALE SUBSIDENCE VARIABILITY

Inspired by the subsidence variability observed in minibasins 7, 9, and 18, we undertook a detailed seismic-stratigraphic analysis of the other 13 minibasins fully imaged within the 3D seismic volume. Our results show that most minibasins contain bowl-shaped packages at their base, indicating most commenced with a phase of broadly symmetrical subsidence (Figs 9 and 10). This phase was typically followed by several phases of asymmetric subsidence, a pattern broadly consistent with models relating the bowl-to-wedge transition to salt welding (Fig. 1A; see also the natural example in Fig. 1C). However, we note that the switch to asymmetric subsidence seemingly occurs at different stages in different minibasins. For example, in some minibasins this switch occurred relatively early (i.e. after only c. 25% of the total minibasin-fill) in their histories (e.g. minibasins 3, 7, 10, 17 and 18; Fig. 10). In contrast, in other minibasins this switch occurred significantly later (e.g. minibasins 4-6, 12-14 and 16), or not at all (e.g. Minibasin 1 is dominated by symmetric subsidence throughout its history; Fig. 10). Additional notable exceptions to the general pattern described above occur in minibasins 2 and 15, where bowl-shaped packages overlie wedge-shaped packages, rather than vice-versa (Fig. 10). The reason for this is unclear, although we discuss possible mechanisms below.

In addition to the relative *timing* of the transition in subsidence style seemingly varying between minibasins, the *direction* of tilting during the asymmetrical subsidence phase was also highly variable. For example, having undergone an initial phase of symmetric subsidence, some minibasins then underwent unidirectional tilting (e.g. minibasins 3, 8, 9 and 12; Fig. 9). In contrast, others minibasins had more complex histories, being defined by either broadly a clockwise (e.g. minibasins 7 and 10) or anticlockwise (e.g. minibasins 7 and 10) rotation of the direction of tilting, or seemingly random jumps in the direction of tilting (e.g. minibasins 1, 2, 13, 15, 18 (Fig. 9).

DISCUSSION

What are the key seismic sequence architectures occurring in minibasins?

'Bowls', 'wedges' and 'layers' (*sensu* Rowan & Weimer, 1998) are the main seismic-stratigraphic geometries mapped in seismically-imaged minibasins in the Precaspian Basin, onshore Kazakhstan. We follow Rowan and Weimer (1998) by inferring that bowls and wedges record symmetric and asymmetric subsidence, respectively, whereas layers document post-welding aggradation of sediment above a minibasin and its flanking diapirs. We show that asymmetric subsidence may be associated with abrupt, relatively large-magnitude changes in the direction of tilting (Figs 7 and 8; see also, for example, minibasin 17 between times '3' and '4', and minibasin 8 between times '2' and '3'; Fig. 9); this, together with post-subsidence shortening and associated tilting of minibasins around a sub-horizontal axis, can lead to unusual seismic-stratigraphic geometries. For example, earlier formed wedges may be rotated to such a degree that stratal units thicken up structural dip (Figs 10A and

11A). At the most basic level, because of this temporally and spatially complex subsidence history, our study shows that simple 2D seismic profiles may not capture the true stratal geometries within minibasins. For example, packages appearing tabular and isopachous in one view, and which seemingly document uniform aggradation, may in fact be wedge-shaped and thicken out-of-plane and instead document strongly asymmetric subsidence (e.g. Unit 3 in minibasin 7; Fig. 7A and D). Thickness maps are therefore essential to accurately capture thickness variations in minibasin stratigraphic packages and constrain the style of minibasin subsidence (cf. Clark et al., 1998).

What controls minibasin subsidence patterns?

Based on when the bowl-to-wedge transitions occurs as a percentage of a minibasins fill, we suggest the switch from symmetrical to asymmetrical subsidence occurred at different times within even closely spaced minibasins. Following the transition to asymmetrical subsidence, and timing uncertainties aside, it is clear that the direction of tilting during the asymmetrical subsidence phase was highly variable. So, what mechanism(s) controlled such temporal and spatial variations in minibasin subsidence in the Precaspian Basin? Answering this question is not straightforward because: (i) Late Cretaceous and Oligo-Miocene regional shortening means the minibasins are now not only closer together than they were immediately post-welding, but also have a different spatial relationship to underlying encased minibasins, which could have impacted how they subsided (see below; see also Duffy et al., 2017; Fernandez et al., 2017); and (ii) a lack of biostratigraphic data mean we cannot constrain when individual minibasins began to subside, nor when asymmetric subsidence commenced. These limitations notwithstanding, based on observations from other salt basins and physical models (see below), and the regional geological evolution of the Precaspian Basin, we now explore some of the mechanisms that may have controlled subsidence patterns here and in other basins.

First, variations in subsidence style may have been controlled by spatial variations in salt thickness and bulk rheology imposed by the latest Permian encased minibasins, a hypothesis we explore with three physical models (Figs 11-14; see also minibasins (i) and (ii) in Fig. 15). Model 1, which replicates purely density-driven subsidence of an isolated minibasin into a ‘sea’ of salt of uniform rheology and thickness (Figs 11A and 12A-B; see also Duffy et al., 2018), shows this minibasin underwent simple symmetric subsidence throughout much of its history. This style of subsidence was recorded by deposition of bowl-shaped stratigraphic packages, with welding indicated by a relatively abrupt upward change to tabular, sub-horizontal packages that extend across flanking diapirs (Fig. 12C). Model 2 also replicates purely density-driven subsidence of a minibasin but, in this case, the underlying salt varies in thickness and bulk rheology due to the presence of encased minibasins (Fig. 11B). The minibasin in Model 2 was nucleated above the flank of an encased minibasin, between an area of thick salt and thin salt above the encased minibasin (Figs 11B and

13A). Spatial changes in salt thickness and bulk rheology mean that the subsidence history of the minibasin in Model 2 was more complex than Model 1. Symmetric subsidence characterised only the earliest stage of minibasin downbuilding in Model 2, as recorded by the deposition of only one or possibly two bowl-shaped packages that, at present, dip west-south-westwards (Fig. 13B-C). Subsequent subsidence was strongly asymmetric, and characterised by west-southwestwards tilting of the minibasin as it subsided more strongly in the area of thick salt; this phase of downbuilding was recorded by deposition of west-southwestwards thickening wedge-shaped packages (Fig. 13C). Most critically, tilting occurred *before* the minibasin welded against the deeper encased minibasins, an interpretation supported by the fact that the combined thickness of bowl-shaped packages (1 cm) at the base of the minibasin is less than the thickness of the underlying salt (2 cm) initially capping the encased minibasin (Fig. 13C). The suprasalt minibasin eventually became too wide to subside through the narrow neck of the feeder, eventually welding against the encased minibasins (Fig. 13B-C). Pre-weld tilting also occurred in Model 3, which explores the effect of a simple, plunging subsalt high on the subsidence patterns of an array of travelling minibasins (Fig. 14). Initial subsidence patterns of all three minibasins were symmetric, defining bowl-shaped sediment packages (Fig. 14A). As the minibasins deepened, salt expulsion from beneath the minibasins began to be impacted by the sub-salt high block, and the perturbed flow caused the minibasins to tilt away from this high block (Fig. 14B). Note that tilting is more pronounced in the northern part of minibasin array where the base-salt relief was higher (Fig. 14B; see also Fig. 11C). Models 2 and 3 broadly replicate the Late Permian-to-Triassic setting of the Precaspian Basin; i.e. suprasalt minibasins subsided through a salt layer of varying thickness, with these variations caused by encased minibasins (Duffy et al., 2017 and Fernandez et al., 2017). In the case of Model 3, subsiding minibasins may have been translating horizontally in response to syn-subsidence shortening (see below) or base-salt tilting. In basins lacking a precursor phase of minibasin formation and encasement, salt thickness variations and complex minibasin subsidence patterns may simply reflect subsalt relief generated by faults or folds (Dooley et al., 2017). In our Precaspian Basin example, late regional shortening means the original spatial relationship between encased and suprasalt minibasins has been modified. This may explain the present lack of a clear spatial relationship between subsidence patterns in the secondary minibasins and the position of encased minibasins (Fig. 9).

Second, lateral differences in the rate of salt expulsion could drive pre-weld tilting and asymmetric subsidence of adjacent minibasins (see minibasins (v) and (vi) in Fig. 14). Such variations in salt expulsion could be triggered by the deposition of relatively dense sediments (e.g., anhydrite, carbonate), or local deposition of thicker and thus denser clastic sequence (e.g. by a point-fed depositional system, such as a delta, or a cluster of deep-water channels; cf. 'sedimentary topographic' loading of Hudec et al. 2009), along one side of a minibasin. More salt will be expelled from the more rapidly subsiding margin, leading to tilting in that direction prior to welding. A local increase in salt flux from beneath the more rapidly subsiding margin of the minibasin may then trigger

tilting of adjacent minibasins away from this location, thus setting up array-scale kinematic interactions (see above and minibasins (v) and (vi) in Fig. 14). This mechanism may be applicable to the Precaspian Basin, given that fluvial clastics and evaporites represent much of the sedimentary fill of the suprasalt (and encased) minibasins (Barde et al. 2002b).

Third, regional shortening can drive minibasin formation, with diapir squeezing and inflation leaving intervening minibasins as bathymetric depressions that can accumulate sediment (Hudec et al., 2009). Subtle differences in the rate of shortening-driven diapir rise may cause minibasin tilting, as minibasins tilt away from more rapidly rising diapirs. Critically, this type of tilting can occur prior to welding (see minibasins (v) and (vi) in Fig. 14). A local increase in salt flux from beneath the more rapidly subsiding margin of the minibasin may also trigger tilting of adjacent minibasins (see above and minibasins (v) and (vi) in Fig. 14). This model may be applicable to the Precaspian Basin, given Uralian Orogeny-related regional shortening likely occurred during Late Permian-to-Triassic subsidence of the suprasalt minibasins (Sokolova et al., 1973; Barde et al., 2002a; Volozh et al., 2003). However, it must be noted there is no direct evidence minibasin initiation or subsidence was coeval with shortening (e.g. presence of thrusts in the deeper parts of the minibasins; Hudec et al., 2009). This may reflect that fact that related shortening strains were buffered by squeezing of relatively wide diapirs.

Finally, minibasin tilting prior to welding could be driven by syn-subsidence lateral translation of minibasins into a lateral buttress (not shown in Fig. 14). In the case of the Precaspian Basin, this buttress would be represented by an encased minibasin. In this context, lateral transition of suprasalt minibasins may have occurred due to syn-subsidence shortening imposed by the Late Permian-to-Triassic, Uralian Orogeny (Sokolova et al., 1973; Barde et al., 2002a; Volozh et al., 2003), or because subsidence occurred in the presence of laterally flowing salt above a regional, broadly W-dipping slope (Fig. 2).

This discussion highlights that several mechanisms may cause minibasin tilting occur prior to welding. As a result, the switch from bowl- to wedge-shaped stratigraphic packages may not record weld timing and the original salt thickness. Future work should focus on examples in which the age and composition of stratigraphy within individual minibasins is better-constrained, and where independent evidence for regional tectonic events is available.

What implications do minibasin subsidence patterns have for hydrocarbon exploration in salt-bearing sedimentary basins?

Halite, which is the most abundant mineral in many salt formations, has a very low permeability (10^{-20} m^2; e.g. Jackson and Hudec, 2017). Thus, depending on their composition (see Wagner and Jackson, 2011; Jackson et al., 2014) the development of salt welds is often critical to allow

transmission of hydrocarbons from subsalt source rocks into suprasalt, minibasin-hosted reservoirs, or between adjacent minibasins (Rowan, 2004; Jackson et al., 2014, 2018). The *timing* of salt welding is also critical (Rowan, 2004); for example, if welding occurs *after* hydrocarbons have been expelled from the source rock, then these hydrocarbons may be either trapped below the salt or may migrate updip into other parts of the subsalt succession. However, if welding occurs *before* hydrocarbon expulsion, then these hydrocarbons may be able to migrate into and charge suprasalt reservoirs. Establishing when welding occurs may thus be of critical importance when exploring for hydrocarbons.

Based on their study of 2D seismic and borehole data from the Gulf of Mexico, Rowan and Weimer (1998) suggest that the transition from bowl- to wedge-shaped seismic sequences may indicate the timing of welding. However, our physical models indicate strongly asymmetric subsidence and minibasin tilting can occur *prior* to welding, and that they may instead document spatial variations in the rate and amount of evacuation of salt from beneath a descending minibasin (e.g. Fig. 4). Furthermore, we speculate that the transition from bowl- to wedge-shaped seismic sequences in the Precaspian Basin may likewise predate welding. Using the timing of the bowl-to-wedge transition to indicate the timing of welding may thus falsely suggest that welding occurred earlier than it really did. The impact of this on exploration risking is clear; if maturation, expulsion and migration of subsalt source rocks occurs prior to welding, than suprasalt reservoir may not be charged, even if, at present, minibasins are welded to subsalt strata. It is thus critical to understand what controls minibasin subsidence style in salt-bearing sedimentary basins when risking, in particular, suprasalt prospects relying on charging from subsalt source rocks.

In addition to constraining (or not constraining) the timing of welding and the likelihood of charging suprasalt reservoirs, the style of minibasin subsidence also controls reservoir distribution. For example, submarine (e.g. Prather et al., 1998; Kane et al., 2012) and fluvial (e.g. Hodgson et al., 1992; Matthews et al., 2009; Banham and Mountney, 2013) channels are typically sensitive to syn-depositional relief, typically being drawn towards bathymetric lows (Fig. 1D), Thus, one may anticipate that reservoirs associated with these systems may occur at specific locations within the three seismic-stratigraphic architectures identified in the Precaspian Basin. For example, channelised reservoirs may occur towards the centre of bowl-shaped sequences (e.g. Hodgson et al., 1992; Matthews et al., 2009; Banham and Mountney, 2013), whereas they may be best-developed at the thicker end of the wedge-shaped sequences, near the salt-sediment contact (Fig. 1D). In contrast, within isopachous layers deposited during long-wavelength, uniform subsidence, these reservoirs may be more evenly distributed across strike. In association with intraformational stratal thinning, onlap and truncation, reservoirs may pinchout updip into sealing lithologies and thus be stratigraphically-trapped towards the thin end of these wedge-shaped packages. Reservoirs in the centres of bowl-shaped seismic sequences may rely on more subtle stratigraphic trapping configurations. The aforementioned discussion is predicated on the fact that the basin is underfilled and that at-surface

relief is developed during minibasin subsidence; e.g. if the minibasin is overfilled, then channel systems may be able to avulse and deposit broader, more sheet-like reservoir elements that are not directly restricted to the location of maximum sediment preservation. In the Precaspian Basin we lack borehole data to test this hypothesis, although it may be testable in other data-rich salt-bearing sedimentary basins (e.g. Gulf of Mexico, North Sea).

CONCLUSIONS

We use 3D seismic reflection data from the Precaspian Basin, onshore Kazakhstan to define the main seismic-scale sequence architectures developed as minibasins subside into salt of varying thickness. We show that bowl-shaped stratigraphic packages are typically overlain by wedge-shaped packages, with the switch between the two recording a change from symmetric to asymmetric subsidence. Asymmetric subsidence may not simply reflect minibasin welding, and the gross thickness of lowermost, bowl-dominated packages may not faithfully record the primary salt thickness; these inferences are consistent with observations from our physical models. The underlying controls on this change in subsidence style remain unclear, although it may reflect lateral variations in salt thickness and bulk rheology, kinematic interactions between adjacent minibasins undergoing non-uniform subsidence at differing rates, and/or syn-subsidence shortening in or without the presence of a lateral buttress. Irrespective of the precise controls on this subsidence variability, the results of our study have important implications for assessing the timing of hydraulic communication between sub-salt, source rock-bearing strata, and suprasalt reservoirs, and for the distribution of suprasalt reservoirs deposited in minibasins.

ACKNOWLEDGEMENTS

We thank Condor Petroleum and especially Roger Whittaker for permission to use and publish seismic reflection and borehole data from the Precaspian Basin. The manuscript was edited by Stephanie Jones. The project was funded by the Applied Geodynamics Laboratory (AGL) Industrial Associates program, comprising the following companies: Anadarko, BHP Billiton, BP, CGGVeritas, Chevron, Cobalt, ConocoPhillips, Ecopetrol, Ente Nazionale Idrocarburi (Eni), ExxonMobil, Fugro, Global Geophysical, Hess, INEXS, Instituto Mexicano del Petróleo (IMP), ION Geophysical, Maersk, Marathon, Mariner, McMoRan, Murphy, Nexen, Noble, Petrobras, Petróleos Mexicanos (PEMEX), Petroleum Geo-Services (PGS), Repsol, Samson, Saudi Aramco, Shell, Equinor, TGS-NOPEC, Total, WesternGeco, and Woodside (http://www.beg.utexas.edu/indassoc/agl/agl_if.html). The authors received additional support from the Jackson School of Geosciences, The University of Texas at Austin. Schlumberger are also thanked for providing Petrel software to The University of Texas at

Austin and Imperial College. Publication authorized by the Director, Bureau of Economic Geology, The University of Texas at Austin.

REFERENCES

Banham, S.G. & Mountney, N.P., 2014. Climatic versus halokinetic control on sedimentation in a dryland fluvial succession. Sedimentology, 61, 570-608.

Barde, J.P., Gralla, P., Harwijanto, J. & Marsky, J., 2002a. Exploration at the eastern edge of the Precaspian basin: Impact of data integration on Upper Permian and Triassic prospectivity. AAPG Bulletin, 86, 399-415.

Barde, J.P., Chamberlain, P., Galavazi, M., Gralla, P., Harwijanto, J., Marsky, J. & van den Belt, F., 2002b. Sedimentation during halokinesis: Permo-Triassic reservoirs of the Saigak field, Precaspian basin, Kazakhstan. Petroleum Geoscience, 8, 177-187.

Brunet, M.-F., Volozh, Y.A., Antipov, M.P. & Lobkovsky, L.I., 1999. The geodynamic evolution of the Precaspian Basin (Kazakhstan) along a north-south section. Tectonophysics, 313, 85-106.

Clark, J.A., Stewart, S.A. & Cartwright, J.A., 1998. Evolution of the NW margin of the North Permian Basin, UK North Sea. Journal of the Geological Society, 155, 663-676.

Davison, I., Anderson, L., & Nuttall, P., 2012. Salt deposition, loading and gravity drainage in the Campos and Santos salt basins. Geological Society, London, Special Publications, 363, 159-174.

Duffy, O.B., Fernandez, N., Hudec, M.R., Jackson, M.P.A., Burg, G., Dooley, T.P. & Jackson, C.A.L., 2017. Lateral mobility of minibasins during shortening: Insights from the SE Precaspian Basin, Kazakhstan. Journal of Structural Geology, 97, 257-276.

Duffy, O.B., Dooley, T.P., Hudec, M.R., Jackson, M.P., Fernandez, N., Jackson, C.A-L. & Soto, J.I., 2018. Structural evolution of salt-influenced fold-and-thrust belts: A synthesis and new insights from basins containing isolated salt diapirs. Journal of Structural Geology, 114, 206-221.

Fernandez, N., Duffy, O.B., Hudec, M.R., Jackson, M.P.A., Burg, G., Jackson, C.A.L. & Dooley, T.P., 2017. The origin of salt-encased sediment packages: Observations from the SE Precaspian Basin (Kazakhstan). Journal of Structural Geology, 97, 237-256.

589 Ge, H., Jackson, M.P.A & Vendeville, B.C., 1997. Kinematics and dynamics of salt tectonics driven
590 by progradation. AAPG Bulletin, 81, 398-423.
591
592 González-Muñoz, J.M., Martín Bañón, J.J. & Carballo-García, J.A., 2001. Salt tectonics and
593 synsedimentary analysis in the southeastern border of the Pre-Caspian basin (Kazakhstan).
594 Exploratory evaluation of potential traps in Permo-Triassic materials. Bol. Inf. Pet., 68 (2001), pp. 84-
595 96
596
597 Gralla, P. & Marsky, J., 2000. Seismic reveals new eastern Precaspian target. Oil & Gas Journal, 98,
598 4.
599
600 Hodgson, N.A., Farnsworth, J. & Fraser, A.J., 1992. Salt-related tectonics, sedimentation and
601 hydrocarbon plays in the Central Graben, North Sea, UKCS. Geological Society, London, Special
602 Publications, 67, 31-63.
603
604 Hudec, M.R. & Jackson, M.P.A., 2007. Terra infirm: understanding salt tectonics. Earth-Science
605 Reviews, 82, 1-28.
606
607 Hudec, M.R., Jackson, M.P.A. & Schultz-Ela, D.D., 2009. The paradox of minibasin subsidence into
608 salt: Clues to the evolution of crustal basins. Geological Society of America Bulletin, 121, 201-221.
609
610 Ismail-Zadeh, A., Wilhelm, H. & Volozh, Y., 2008. Geothermal evolution of the Astrakhan arch
611 region of the Pricaspian basin. Int. J. Earth Sci., 97, 1029-1043.
612
613 Jackson, M.P.A. & Cramez, C., 1989. Seismic recognition of salt welds in salt tectonic regimes.
614 Proceedings of the GCSSEPM Foundation 10th Annual Bob F. Perkins Research Conference, 66-71.
615
616 Jackson, M.P. and Hudec, M.R., 2017. Salt Tectonics: Principles and Practice. 408 Cambridge
617 University
618 409 Press.
619
620 Jackson, M.P.A. & Talbot, C.J., 1991. A glossary of salt tectonics. University of Texas at Austin,
621 Bureau of Economic Geology Geologic Circular, 91, 44 p.
622
623 Jackson, C.A.L., Jackson, M.P.A. & Hudec, M.R., 2015. Understanding the kinematics of salt-bearing
624 passive margins: A critical test of competing hypotheses for the origin of the Albian Gap, Santos
625 Basin, offshore Brazil. Geological Society of America Bulletin, 127, 1730-1751.

Kane, I.A., McGee, D.T. & Jobe, Z.R., 2012. Halokinetic effects on submarine channel equilibrium profiles and implications for facies architecture: conceptual model illustrated with a case study from Magnolia Field, Gulf of Mexico. Geological Society, London, Special Publications, 363, 289-302.

Prather, B.E., 2000. Calibration and visualization of depositional process models for above-grade slopes: a case study from the Gulf of Mexico. Marine and Petroleum Geology, 17, 619-638.

Prather, B.E., Booth, J.R., Steffens, G.S. & Craig, P.A., 1998. Classification, lithologic calibration, and stratigraphic succession of seismic facies of intraslope basins, deep-water Gulf of Mexico. AAPG Bulletin, 82, 701-728.

Rowan, M.G., 2004. Do salt welds seal? Proceedings of the GCSSEPM Foundation 24th Annual Bob F. Perkins Research Conference (Salt-Sediment Interactions and Hydrocarbon Prospectivity: Concepts, Applications, and Case Studies for the 21st Century), 390-403.

Rowan, M.G. & Weimer, P., 1998. Salt-sediment interaction, northern Green Canyon and Ewing bank (offshore Louisiana), northern Gulf of Mexico. AAPG Bulletin, 82,1055-1082.

Sokolova, E.I., Lipatova, V.V., Starozhilova, N.N., Schleifer., A.G., 1973. Upper Permian and Triassic deposits of the Caspian (Prikaspiyskaya) depression. Permian Triassic Systems and Their Mutual Boundary, 2, 158-167.

Matthews, W.J., Hampson, G.J., Trudgill, B.D. & Underhill, J.R., 2007. Controls on fluviolacustrine reservoir distribution and architecture in passive salt-diapir provinces: Insights from outcrop analogs. AAPG Bulletin, 91, 1367-1403.

Volozh, Y., Talbot, C. & Ismail-Zadeh, A., 2003a. Salt structures and hydrocarbons in the Pricaspian basin. AAPG Bulletin, 87, 313-334.

Volozh, Y.A., Antipov, M., Brunet, M-F., Garagash, I., Lobkovskii, L. & Cadet, J.P., 2003b, Pre-Mesozoic geodynamics of the Precaspian basin (Kazakhstan). Sedimentary Geology, 156, 35-58.

Worrall, D.M. & Snelson, S., 1989. Evolution of the northern Gulf of Mexico, with emphasis on Cenozoic growth faulting and the role of salt. In: The Geology of North America—an overview (Eds. in Bally, A.W. & Palmer, A.R). Boulder, Colorado, Geological Society of America, v. A, 97–138.

663 **FIGURE CAPTIONS**

664

665 **Fig. 1.** (A) Development of bowl (B), wedge (W) and layer (L) stratigraphic/seismic-stratigraphic
666 units during minibasin subsidence and passive diapirism (terminology after Rowan and Weimer,
667 1998). Note progressive shifts in the axis of subsidence associated with welding and the transition
668 from a primary (stages I and II) to secondary (stages III-IV) peripheral sink (*sensu* Trusheim, 1960).
669 No scale implied. (B) Depth-migrated seismic section from the Gulf of Mexico showing the seismic-
670 stratigraphic architecture of a Plio-Pleistocene minibasin forming due to subsidence into
671 allochthonous salt. Vertical stacking of bowl-shaped (B) sequences, at least in this two-dimensional
672 profile, documents vertical, broadly symmetrical minibasin subsidence. Modified from Hudec et al.
673 (2009). (C) Geoseismic section (from a time-migrated seismic profile) showing an overall upward
674 transition from bowl- (B) to wedge-shaped (W) seismic sequences in a Plio-Pleistocene minibasins,
675 again subsiding into allochthonous salt in the Gulf of Mexico. Note the abrupt southward shift in
676 depocentre location (between the light-blue and dark-green layers), which is inferred to document the
677 onset of minibasin welding onto subsalt strata. The potential location of deep-water channels is
678 schematically shown, indicating these types of reservoir are likely to occur where syn-depositional
679 subsidence was greatest. Modified from Rowan and Weimer (1998). (D) Abrupt shifts in minibasin
680 depocentre location due to syn-subsidence shortening. An early bowl-shaped (B) depocentre (light-
681 blue) is almost completely dissected by a post-depositional thrust, which segments the early
682 depocentre into two depocentres (recorded by two bowls (B); green) separated by a thrust-cored high.
683 Asymmetric subsidence (recorded by a wedge-shaped (W) sequence; tan) then occurs due to ongoing
684 shortening, which causes the right-hand diapir to inflate more rapidly than the one on the left. Note
685 that this complex seismic sequence architecture occurs prior to welding (cf. Fig. 1A and C). Modified
686 from Hudec et al. (2009). (E) Abrupt shifts in depocentre location and strongly asymmetric minibasin
687 subsidence recorded by isopachs, western Platform, North Sea. In this setting, differential subsidence
688 occurred *during* rather than after salt, likely due to syn-salt deposition of dense anhydrite and
689 carbonate on less dense halite. Modified from Clark et al. (1998).

690

691 **Fig. 2.** (A) Salt thickness and structure map of Precaspian Basin. Modified from Volozh et al.
692 (2003a). Regional geographic context is shown in the inset map. Study area is shown by a black box
693 located in the SE corner of the basin. Approximate location of section shown in (B) is indicated. (B)
694 Broadly ESE-trending cross-section through the SE margin of the Precaspian Basin. The main
695 tectono-stratigraphic and salt-tectonic features are indicated. The approximate location of the study
696 area is indicated. The approximate location of the cross-section is shown in (A).

697

698 **Fig. 3.** Stratigraphic framework and representative lithologies of key units in the Eastern Precaspian
699 Basin. Modified from Barde et al. (2002b). Key seismic horizons and seismic sequences shown in

subsequent figures are indicated (i.e. Figs 5-8). Key tectonic events and phases of inferred salt mobilisation also shown.

Fig. 4. (A) Structure map of top allochthonous salt showing the distribution of key salt-tectonic features within the study area (i.e. diapirs and minibasins; see also Fig. 5). Location of the seismic and geoseismic sections shown in Fig. 5 is indicated. (B) Structure map of top of encased minibasins fully or partly overlain by allochthonous salt (see Fig. 5) (see Duffy et al., 2017 and Fernandez et al., 2017). Stars mark borehole locations. (C) Simplified map compiled from (A) and (B) showing the location of salt diapirs, and encased and suprasalt minibasins. V-Z are encased minibasins referred to in the text, and labelled in Figs 7, 8 and 12. The locations of maps shown in Figs 6-8 are shown.

Fig. 5. (A) Uninterpreted and (B) interpreted seismic section (from the depth-migrated volume used by Duffy et al., 2017 and Fernandez et al., 2017) showing main structural elements of within the study area. Paired black dots labelled 'p' and 't' are (apparent; (*sensu* Wagner and Jackson, 2011) primary and tertiary salt welds, respectively. Location of the profile is shown in Fig. 4A.

Fig. 6. (A) E-trending seismic profile across minibasin 9 (for location of see Fig. 6B; for location of minibasin see Fig. 4C). Key regional seismic horizons are labelled (BJU=yellow; BCU=orange). White horizons are locally mapped within this minibasin, where they define boundaries between seismic sequences discussed in the text. The stratigraphic positions of isochrons shown in (B-E) are indicated. (B) Unit 1 isochron. (C) Unit 2 isochron. (D) Unit 3 isochron. (E) Unit 4 isochron. Numbers in (B) refer to minibasins named in Fig. 4C. Black dots in (B)-(E) indicate depositional maxima and inferred loci of maximum subsidence. Contour interval=50 ms (TWT).

Fig. 7. (A) E-trending seismic profile across minibasin 7 (for location see Fig. 7B; for location of minibasin see Fig. 4C). Key regional seismic horizons are labelled (BJU=yellow; BCU=orange). White horizons are locally mapped within this minibasin, where they define boundaries between seismic sequences discussed in the text. The stratigraphic positions of isochrons shown in (B-E) are indicated. W is the encased minibasin referred to in the text, and seen in (A) and Fig. 4C. (B) Unit 1 isochron. (C) Unit 2 isochron. (D) Unit 3 isochron. (E) Unit 4 isochron. (F) Unit 5 isochron. Numbers in (B) refer to minibasins named in Fig. 4C. Black dots in (B)-(F) indicate depositional maxima and inferred loci of maximum subsidence. Contour interval=50 ms (TWT).

Fig. 8. (A) E-trending seismic profile across minibasin 18 (for location see Fig. 8B; for location of minibasin see Fig. 4C). Key regional seismic horizons are labelled (BJU=yellow; BCU=orange). White horizons are locally mapped within this minibasin, where they define boundaries between seismic sequences discussed in the text. The stratigraphic positions of isochrons shown in (B-E) are

indicated. IMB=intra-minibasin diapir (see text). X and Y are the encased minibasins referred to in the text, and seen in (A) and Fig. 4C. (B) Unit 1 isochron. (C) Unit 2 isochron. (D) Unit 3 isochron. (E) Unit 4 isochron. Numbers in (B) refer to minibasins named in Fig. 4C. Black dots in (B)-(E) indicate depositional maxima and inferred loci of maximum subsidence. Contour interval=50 ms (TWT).

Fig. 9. Map showing minibasin subsidence patterns across much of the array shown in Fig. 4A and C. Minibasins 1, 6, 11, 16, 19, 20 and 22 were only partly imaged in our 3D seismic volume and were thus not studied. Numbers show the locations of depocentre defined by seismic sequence thickness mapped in individual minibasins; no temporal linked between seismic sequences between minibasins is implied. Black arrows point in the direction of inferred salt evacuation; this is based on the direction of wedge-thickening, which we infer defines the syn-depositional locus of maximum subsidence and hence salt expulsion. V-Z are encased minibasins referred to in the text, and labelled in Figs 4, 7 and 8.

Fig. 10. Chart showing how the distribution of bowl-, wedge-, and layer-shaped seismic-stratigraphic packages vary across the minibasin array, and how their relative thickness vary between minibasins. All minibasins are welded to presalt strata and, in some cases, encased minibasins. Minibasin thickness is calculated from its basal weld to the base Jurassic Unconformity, and is based on true stratigraphic thicknesses to account for severe tilting of earliest deposited strata. The majority of stratigraphic transitions between bowl- and wedge-shaped packages are abrupt, although transitional boundaries are locally observed. For detailed analysis of minibasin 7, 9, and 18 see Figs. 7, 6, and 8, respectively. Maps in Fig. 4B-C indicate the density of encased minibasins as referred to here.

Fig. 11. Initial set-up of physical models. (A) Model 1 (isolated minibasin subsiding in a sea of tabular salt). (B) Model 2 (isolated minibasin subsiding in a salt layer of varying thickness). See text for full discussion. (C) Model 3 (eastward-travelling, isolated minibasins in a sea of salt that changes in thickness along a subsalt high). Note that in (C) base-salt is tilted and salt flow is away from the viewer (see Fig. 14).

Fig. 12. Results of Model 1. (A) Initial minibasin seed within a sea of tabular salt (see also Fig. 11A). Note that a light dusting of blue sand covers the salt to permit laser-scanning of its top surface. (B) Depth slice through the model, the location of which is shown in (C). Strata are sub-horizontal, except at the minibasin margins where it is upturned against the flanking salt diapir. (C) Cross-sections (i and ii) through the model, the locations of which is shown in (B). Note the dominance of bowl- (B) and layer-shaped (L) stratal units below and above, respectively, the horizon marked ‘X’; this stratigraphic transition defines the timing of welding.

Fig. 13. Results of Model 2. (A) Initial (suprasalt) minibasin seed offset from the locus of thick salt within a diapiric feeder (see also Fig. 11B). (B) Depth slice through the model, the location of which is shown in (C). Note the minibasin is almost fully welded, via lateral welds, to the encased minibasins (see also C). Strata dip west-southwestwards, towards the area of thick salt within the diapiric feeder. (C) Cross-sections (i and ii) through the model, the locations of which is shown in (B). A very thin interval of bowl-shaped packages is only developed at the minibasin base below the horizon marked 'Y'; above this level, wedge-shaped packages dominate.

Fig. 14. Results of Model 3 shown as height-change maps of the model top surface. Model tilt, salt flow, and minibasin travel are to the east, towards the southward-plunging subsalt high. Salt is thicker above the southern end of the subsalt high (see Fig. 11C for cross-section through model set-up). (A) Early stage of the model run, in which the white dots indicate the locus of minibasin subsidence; and (B) late stage of the model run, in which the white dots indicate the current locus of minibasin subsidence and the red dots the earlier locus of minibasin subsidence. Note the switch from symmetrical to asymmetrical subsidence, with backtilting of the minibasins away from the subsalt high.

Fig. 15. Simplified conceptual diagrams illustrating some of the key controls on minibasin subsidence styles, based on observations from the Precaspian Basin and the physical models shown in Figs 11-13. Minibasins nucleate above base-salt highs (i.e. encased minibasins in the case of minibasins (i) and (ii), and a subsalt horst in the case of minibasin (iii)), away from base-salt highs and other minibasins (i.e. minibasin (iv)), or in close proximity to one another, but away from base salt highs (i.e. minibasins (v) and (vi)). Note that minibasin subsidence is occurring simply in response to density-driven downbuilding and passive diapiric rise; no horizontal shortening is imposed. Horizontal shortening could however enhance differential salt evacuation from below and diapir rise adjacent to minibasins (v) and (vi). Note also that minibasins (iv) and (v) are too far apart to kinematically interact, in contrast to (v) and (vi). See text for full discussion.

Fig. 1

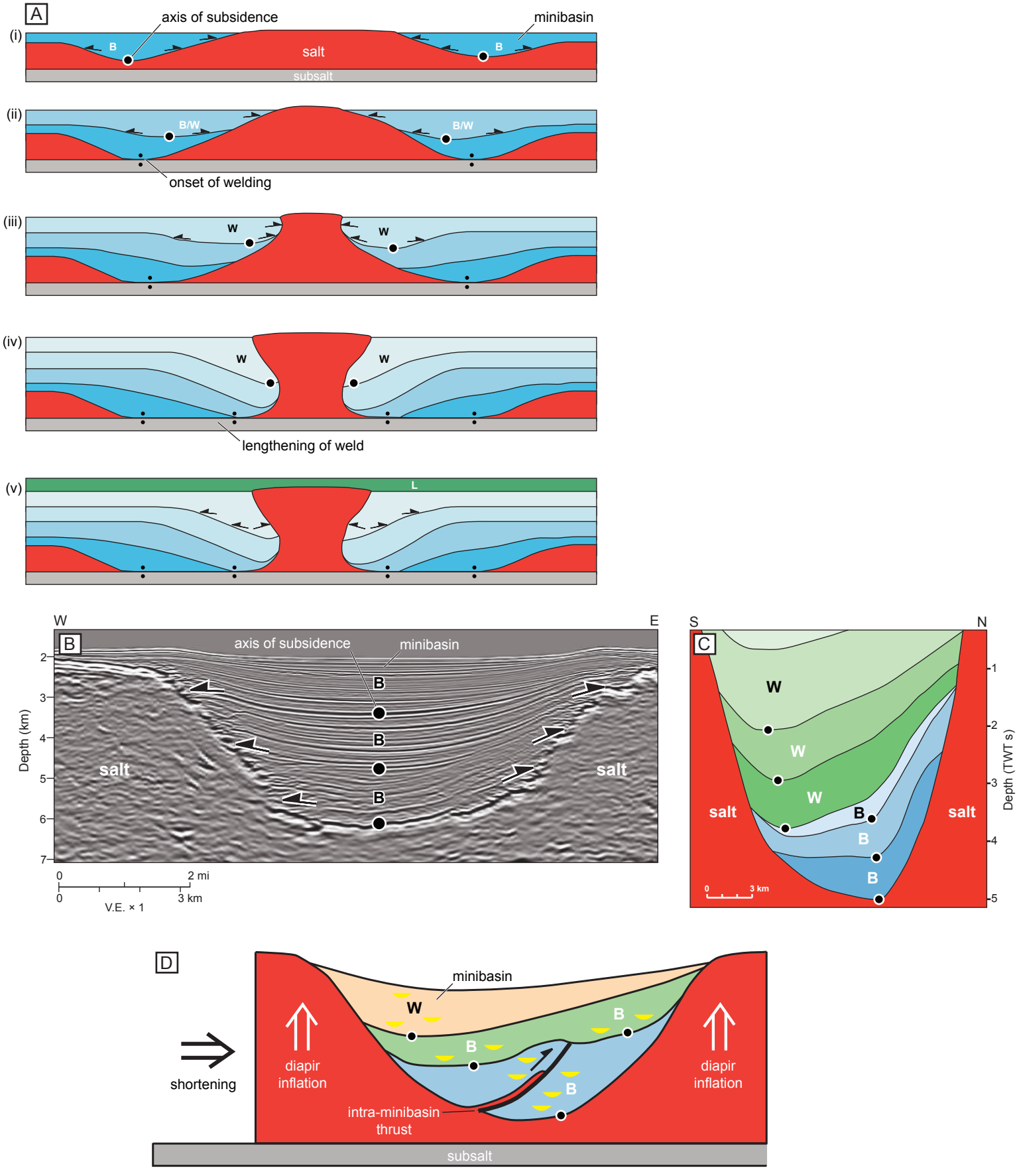
A
(i)
axis of subsidence
minibasin
B
salt
B
subsalt
(ii)
B/W
B/W
onset of welding
(iii)
W
W
(iv)
W
W
lengthening of weld
(v)
L
W
E
B
axis of subsidence
minibasin
B
B
B
salt
salt
Depth (km)
2
3
4
5
6
7
0
2 mi
0
3 km
V.E. × 1
S
N
C
W
W
W
salt
salt
B
B
B
0
3 km
Depth (TWT s)
1
2
3
4
5
D
minibasin
W
B
B
B
shortening
diapir
inflation
diapir
inflation
intra-minibasin
thrust
subsalt

Fig. 1

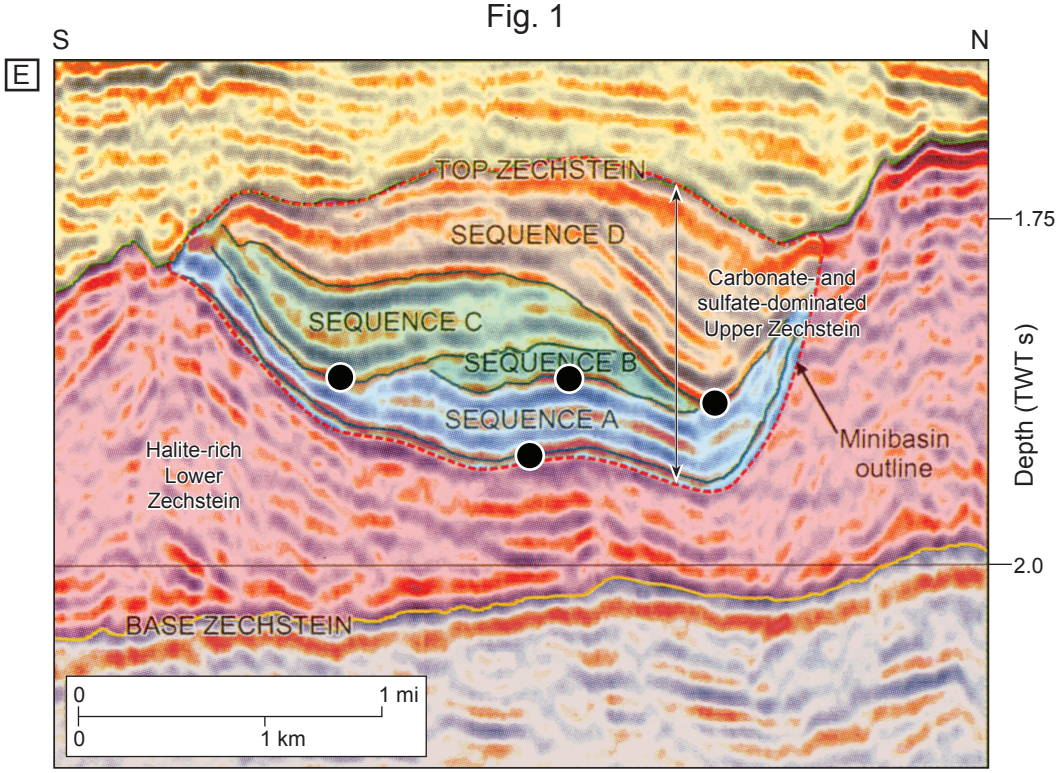
E
S
N
TOP ZECHSTEIN
SEQUENCE D
SEQUENCE C
SEQUENCE B
SEQUENCE A
Carbonate- and sulfate-dominated Upper Zechstein
Minibasin outline
Halite-rich Lower Zechstein
BASE ZECHSTEIN
1.75
2.0
Depth (TWT s)
0
1 mi
0
1 km

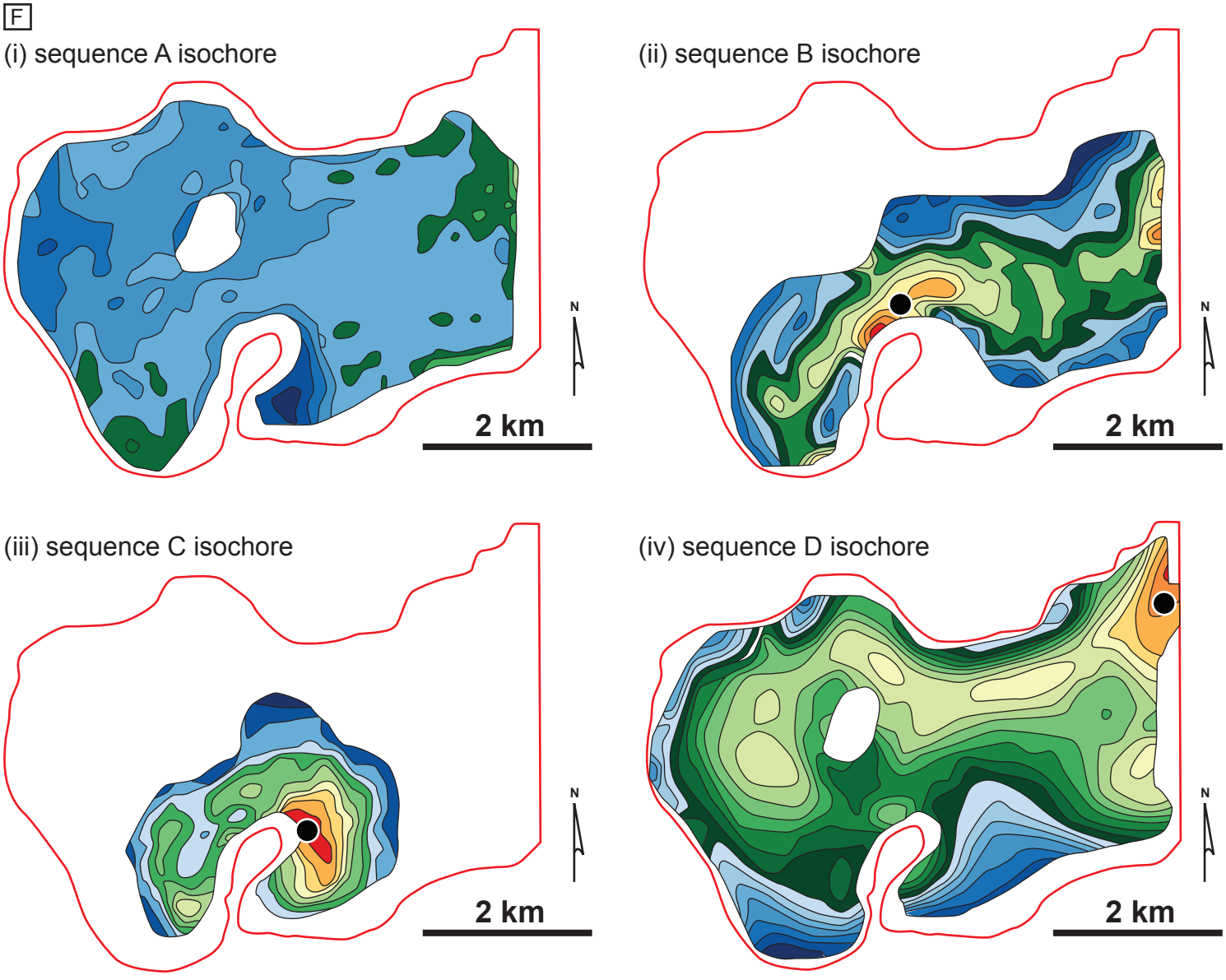
F
(i) sequence A isochore
(ii) sequence B isochore
(iii) sequence C isochore
(iv) sequence D isochore
N
2 km

Fig. 2

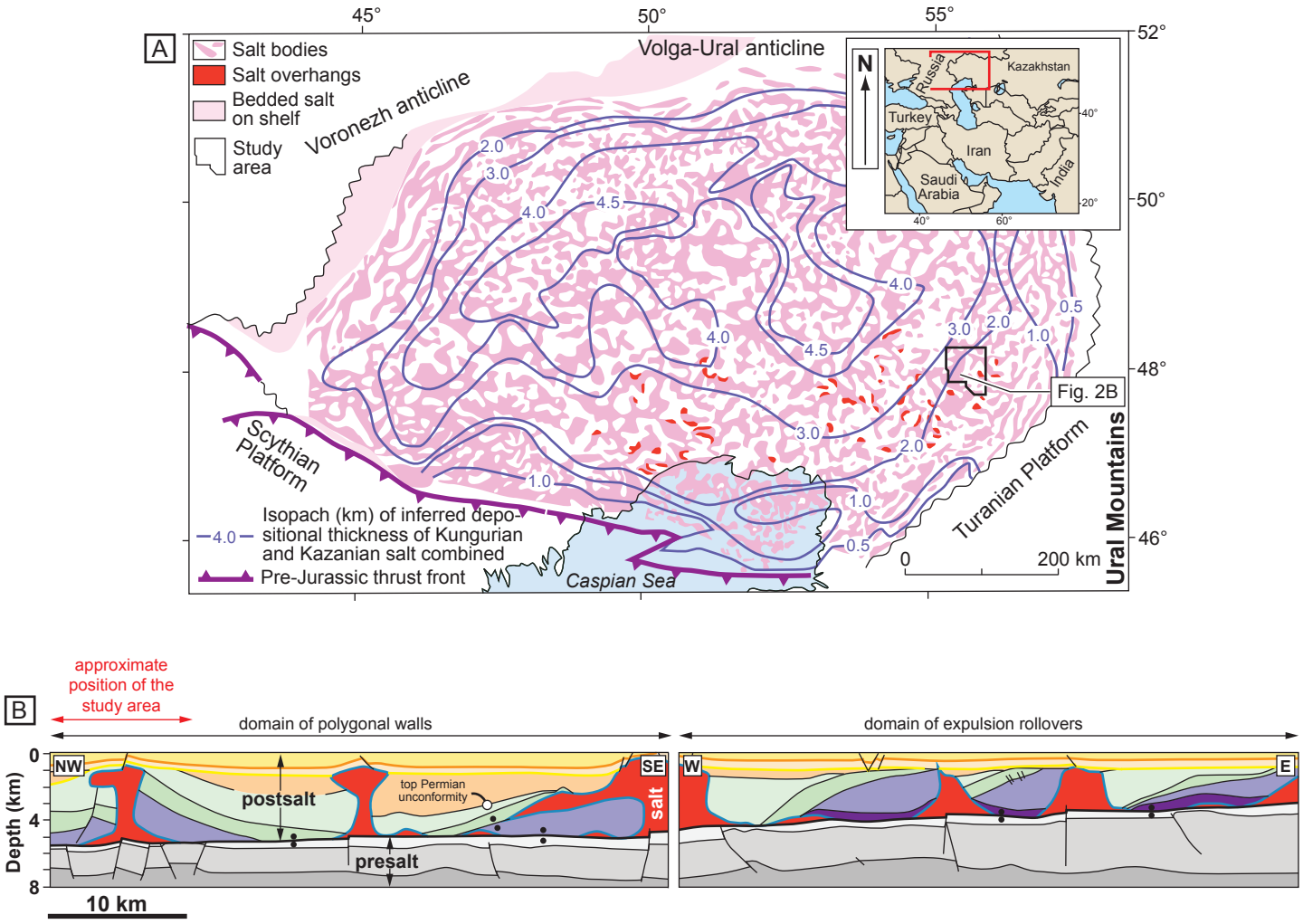
A
45°
50°
55°
52°
50°
48°
46°
Salt bodies
Salt overhangs
Bedded salt on shelf
Study area
Volga-Ural anticline
Voronezh anticline
Scythian Platform
Turanian Platform
Ural Mountains
Caspian Sea
Fig. 2B
Isopach (km) of inferred depositional thickness of Kungurian and Kazanian salt combined
Pre-Jurassic thrust front
0
200 km
N
Russia
Kazakhstan
Turkey
Iran
Saudi Arabia
India
40°
60°
20°
B
approximate position of the study area
domain of polygonal walls
domain of expulsion rollovers
NW
SE
W
E
postsalt
presalt
top Permian unconformity
salt
Depth (km)
0
4
8
10 km

Fig. 3

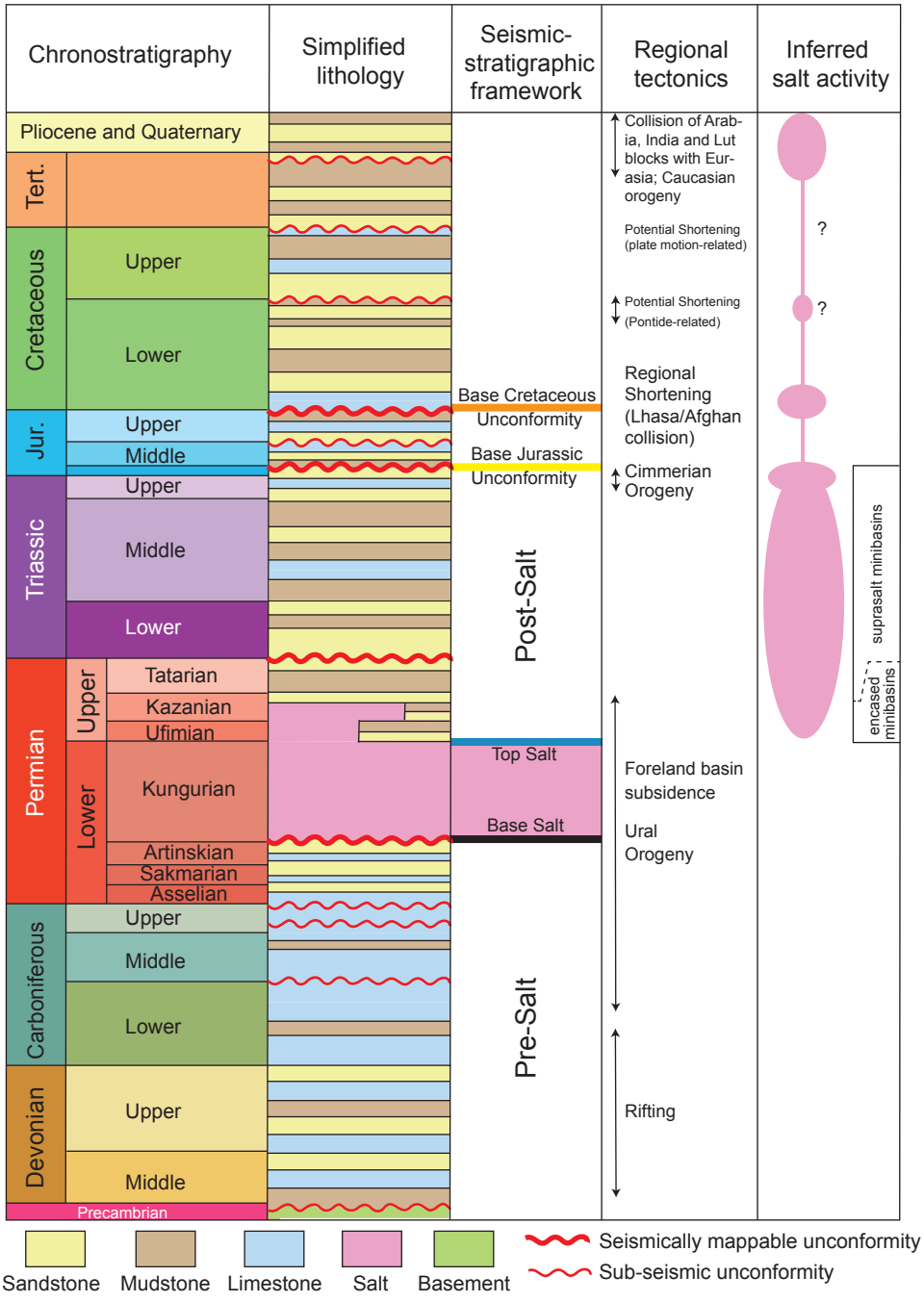
Chronostratigraphy
Simplified lithology
Seismic-stratigraphic framework
Regional tectonics
Inferred salt activity
Pliocene and Quaternary
Tert.
Cretaceous
Upper
Lower
Jur.
Upper
Middle
Triassic
Upper
Middle
Lower
Permian
Upper
Tatarian
Kazanian
Ufimian
Lower
Kungurian
Artinskian
Sakmarian
Asselian
Carboniferous
Upper
Middle
Lower
Devonian
Upper
Middle
Precambrian
Base Cretaceous Unconformity
Base Jurassic Unconformity
Post-Salt
Top Salt
Base Salt
Pre-Salt
Collision of Arabia, India and Lut blocks with Eurasia; Caucasian orogeny
Potential Shortening (plate motion-related)
Potential Shortening (Pontide-related)
Regional Shortening (Lhasa/Afghan collision)
Cimmerian Orogeny
Foreland basin subsidence
Ural Orogeny
Rifting
?
?
suprasalt minibasins
encased minibasins
Sandstone
Mudstone
Limestone
Salt
Basement
Seismically mappable unconformity
Sub-seismic unconformity

Fig. 4

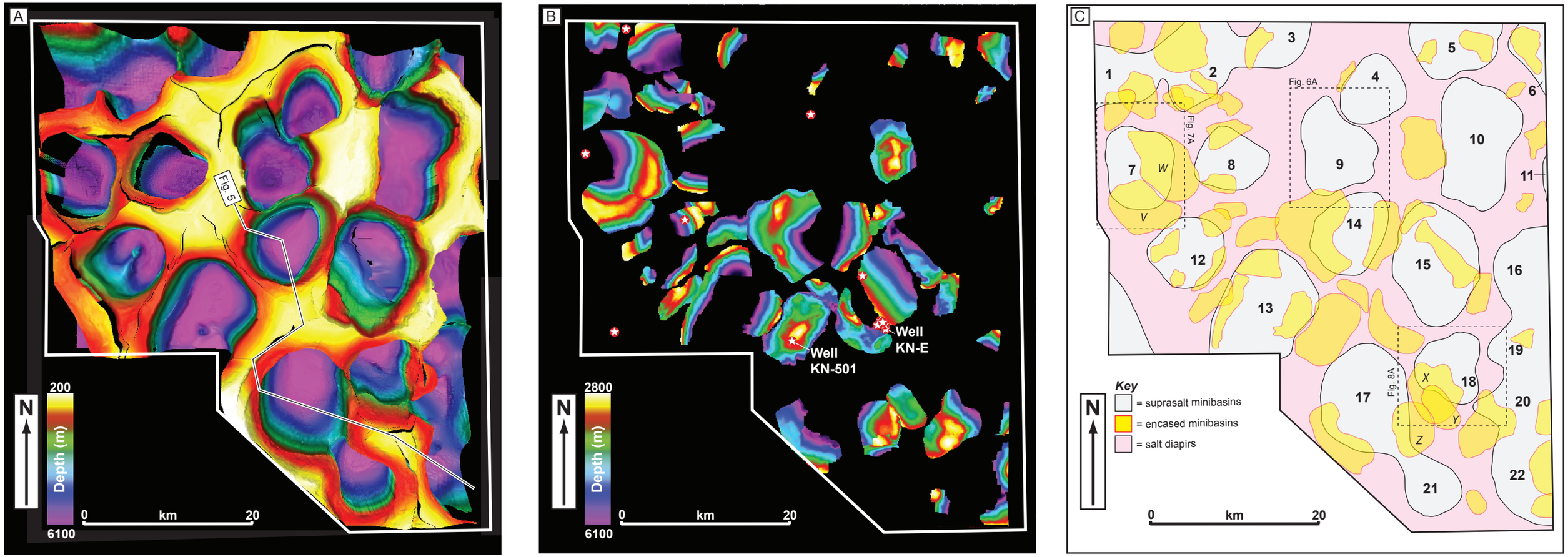
A
Fig. 5
N
200
Depth (m)
6100
0
km
20
B
Well
KN-501
Well
KN-E
N
2800
Depth (m)
6100
0
km
20
C
1
2
3
4
5
6
7
8
9
10
11
12
13
14
15
16
17
18
19
20
21
22
Fig. 6A
Fig. 7A
Fig. 8A
W
V
X
Y
Z
Key
= suprasalt minibasins
= encased minibasins
= salt diapirs
N
0
km
20

Fig. 5

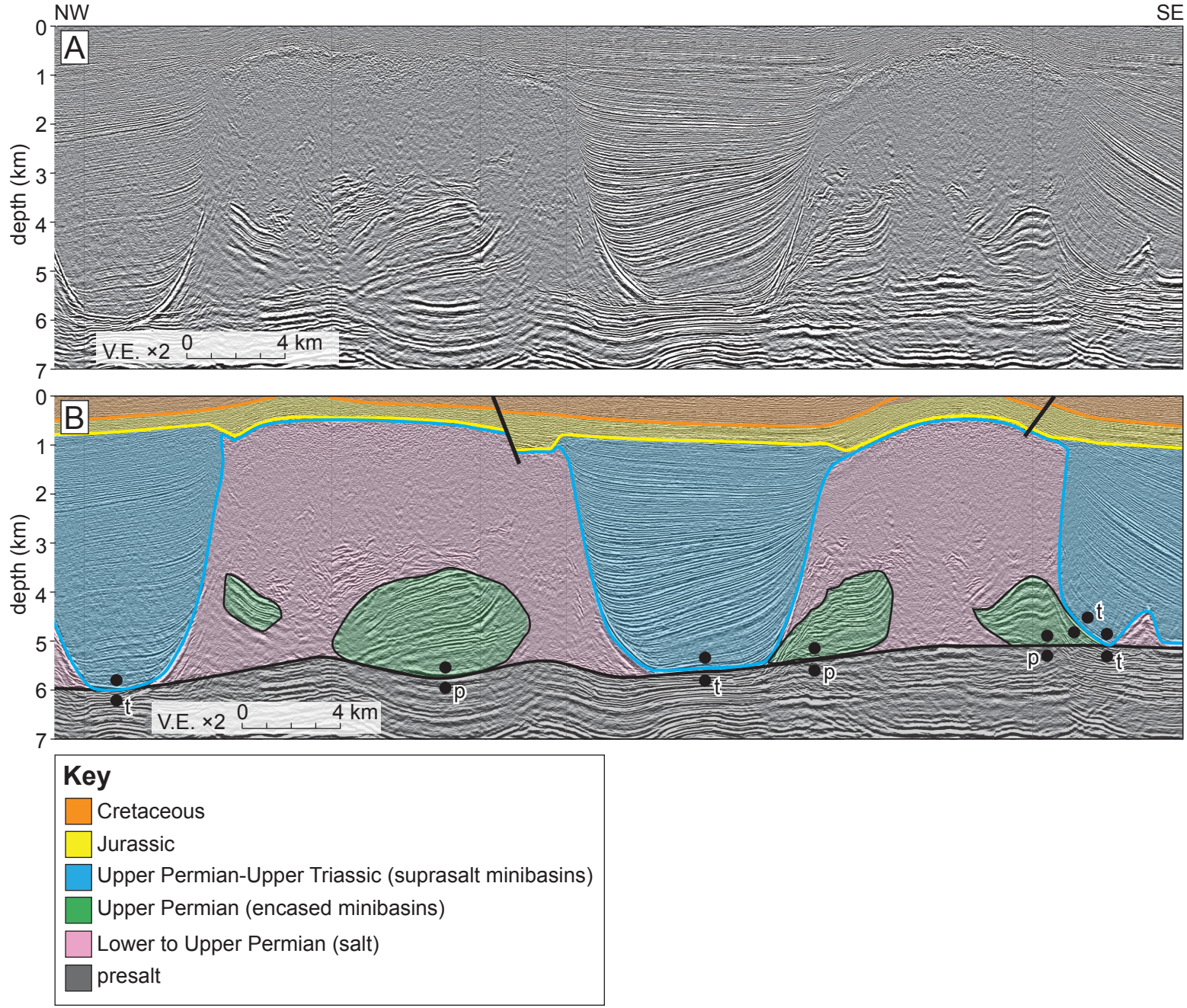
NW
SE
A
B
depth (km)
0
1
2
3
4
5
6
7
V.E. ×2
0
4 km
t
p
Key
Cretaceous
Jurassic
Upper Permian-Upper Triassic (suprasalt minibasins)
Upper Permian (encased minibasins)
Lower to Upper Permian (salt)
presalt

Fig. 6

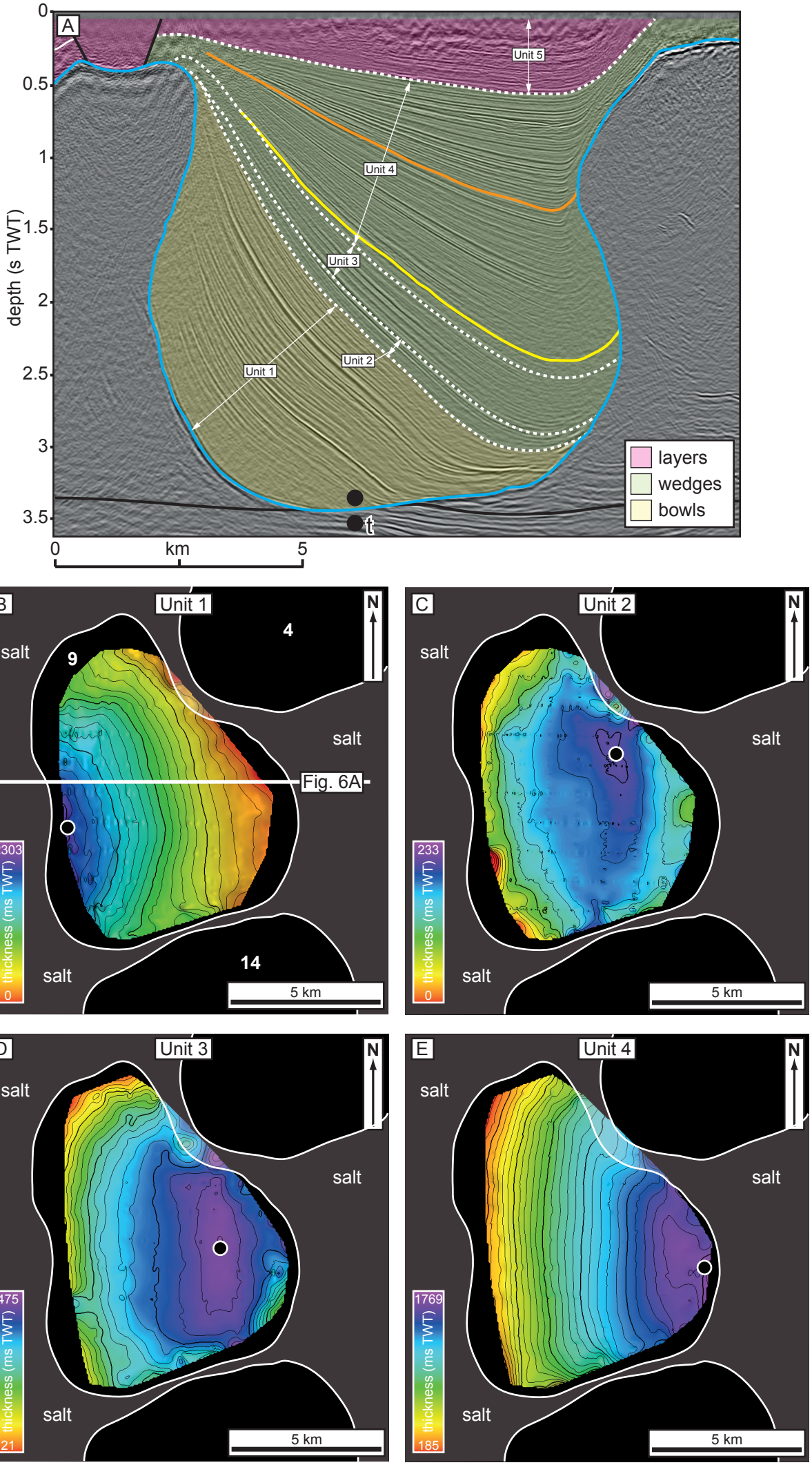
A
Unit 5
Unit 4
Unit 3
Unit 2
Unit 1
depth (s TWT)
0
0.5
1
1.5
2
2.5
3
3.5
0
km
5
layers
wedges
bowls
t
B
Unit 1
N
4
salt
9
salt
Fig. 6A
2303
thickness (ms TWT)
0
salt
14
5 km
C
Unit 2
N
salt
salt
233
thickness (ms TWT)
0
salt
5 km
D
Unit 3
N
salt
salt
475
thickness (ms TWT)
21
salt
5 km
E
Unit 4
N
salt
salt
1769
thickness (ms TWT)
185
salt
5 km

Fig. 7

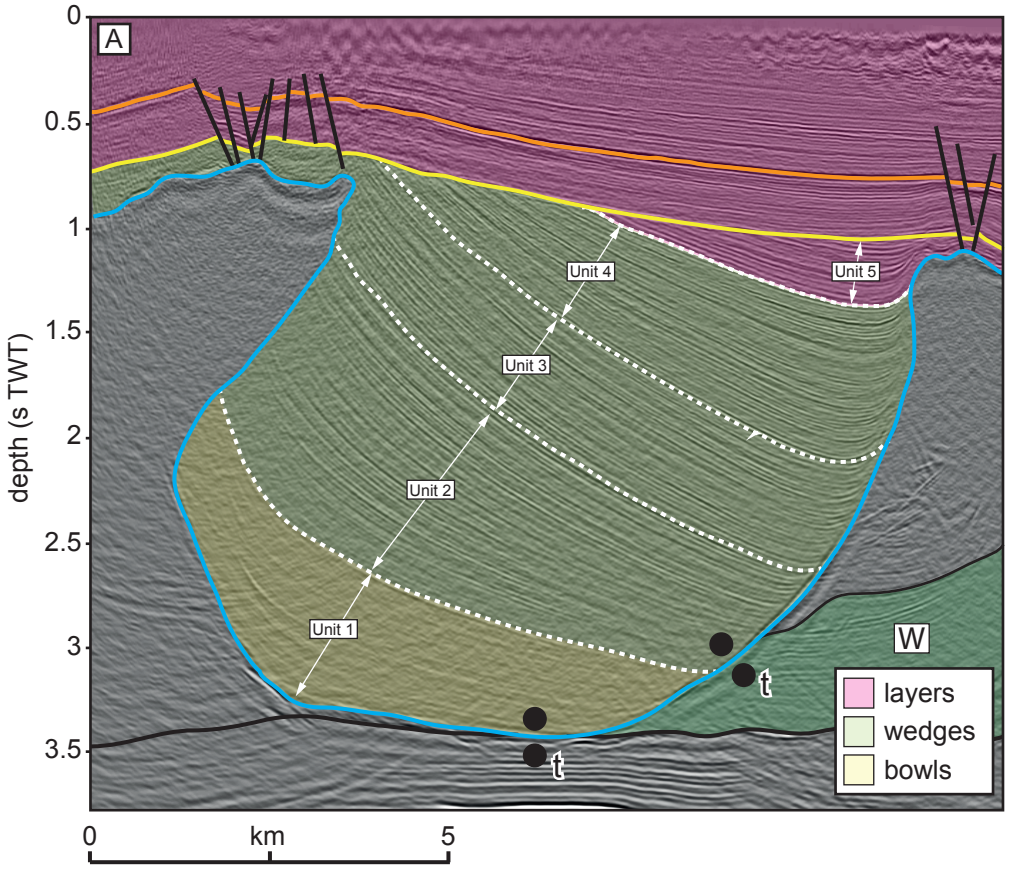
A
depth (s TWT)
0
0.5
1
1.5
2
2.5
3
3.5
Unit 1
Unit 2
Unit 3
Unit 4
Unit 5
W
t
t
layers
wedges
bowls
0
km
5

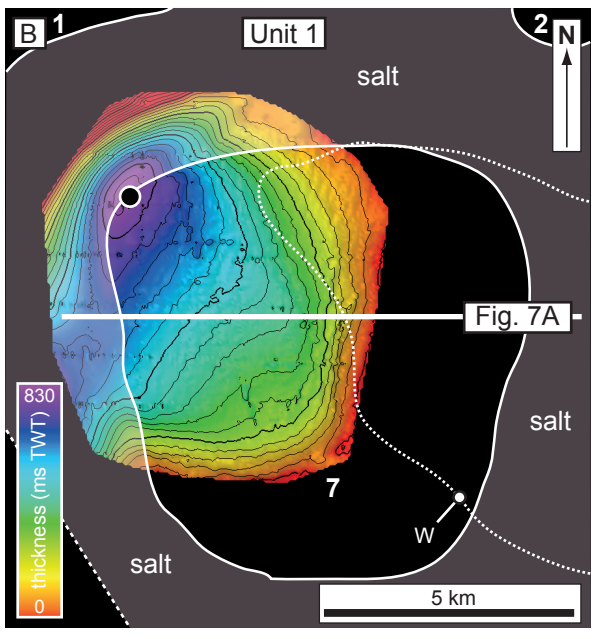
B
Unit 1
1
2
N
salt
salt
salt
Fig. 7A
7
W
830
thickness (ms TWT)
0
5 km

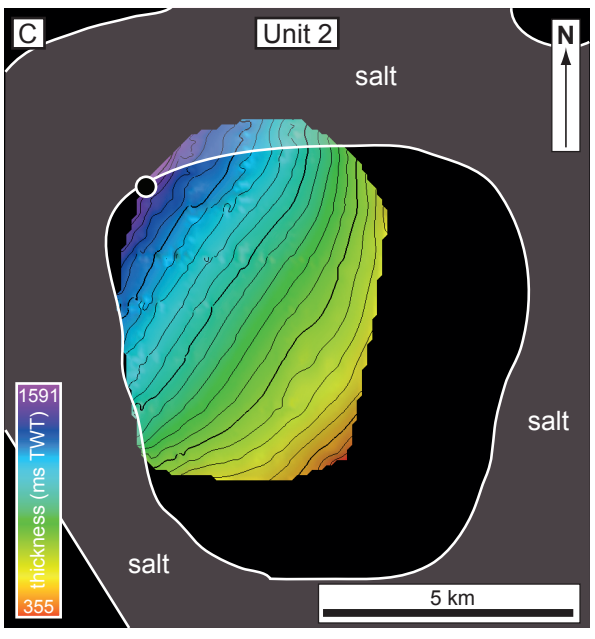
C
Unit 2
N
salt
salt
salt
1591
thickness (ms TWT)
355
5 km

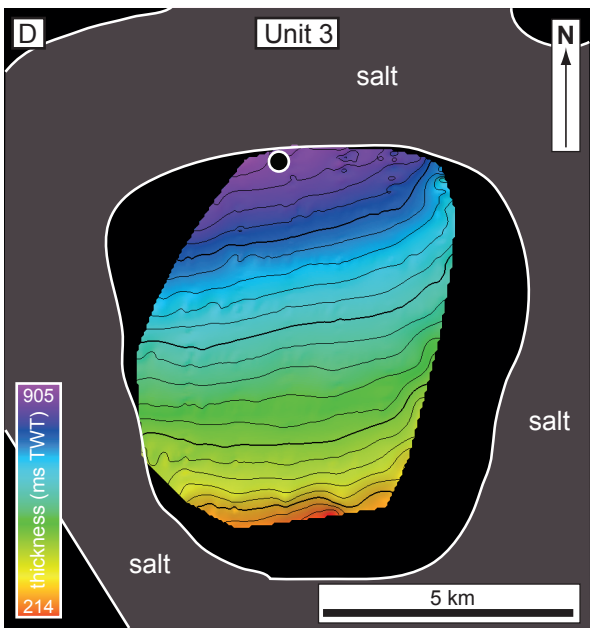
D
Unit 3
N
salt
salt
salt
905
thickness (ms TWT)
214
5 km

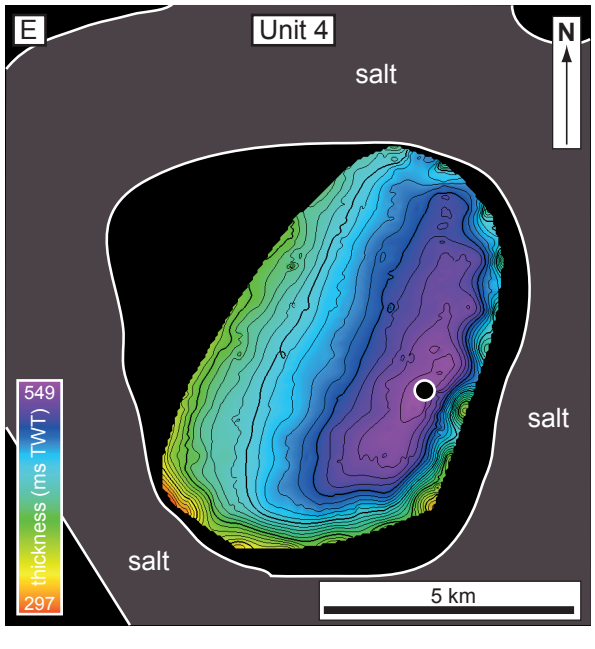
E
Unit 4
N
salt
salt
salt
549
thickness (ms TWT)
297
5 km

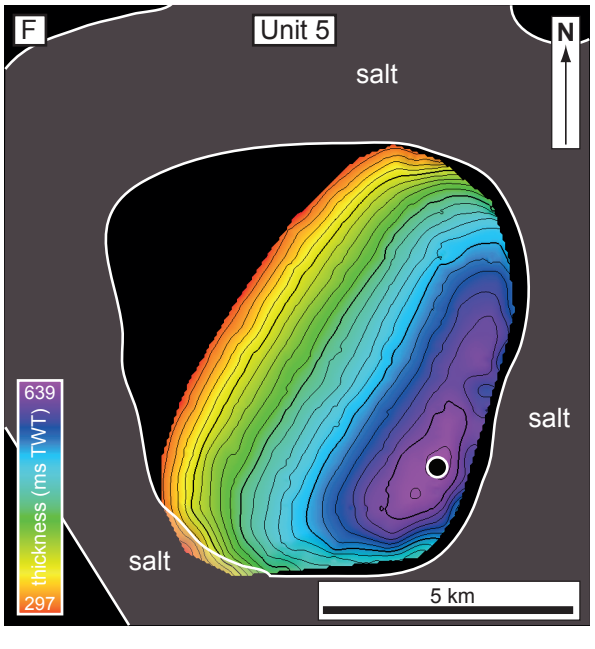
F
Unit 5
N
salt
salt
salt
639
thickness (ms TWT)
297
5 km

Fig. 8

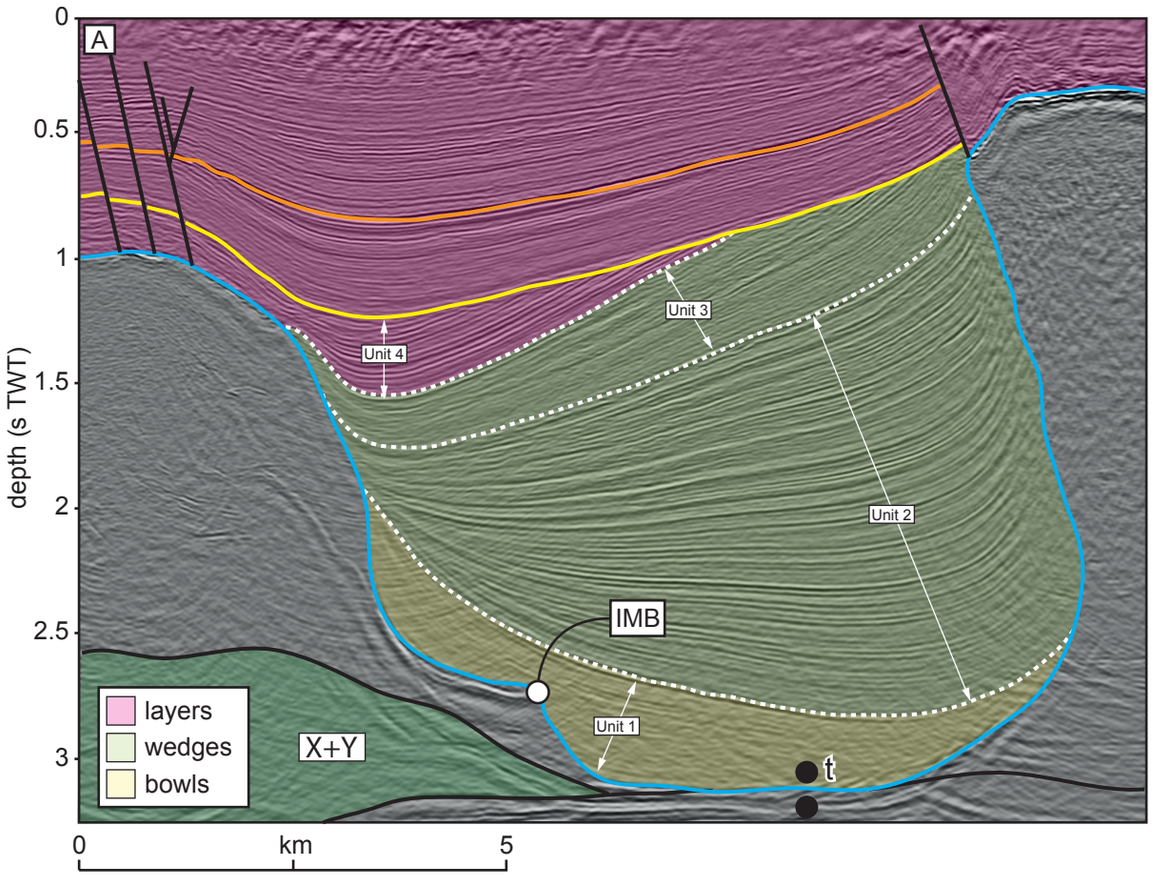
A
depth (s TWT)
0
0.5
1
1.5
2
2.5
3
Unit 4
Unit 3
Unit 2
Unit 1
IMB
t
layers
wedges
bowls
X+Y
0
km
5

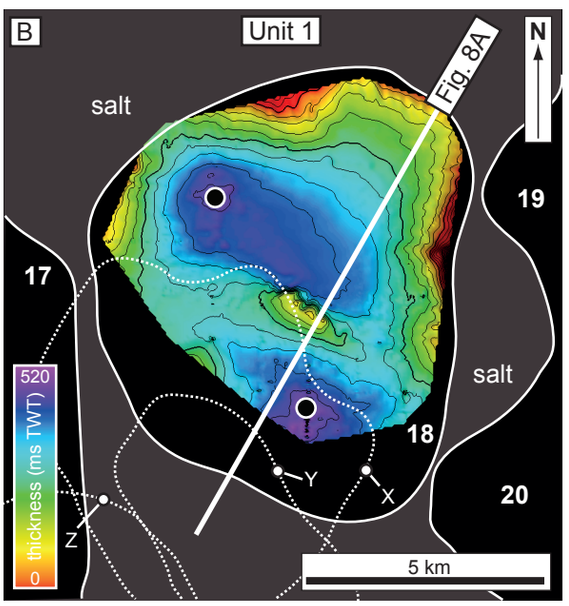
B
Unit 1
N
Fig. 8A
salt
17
19
18
20
520
thickness (ms TWT)
0
Y
X
Z
5 km

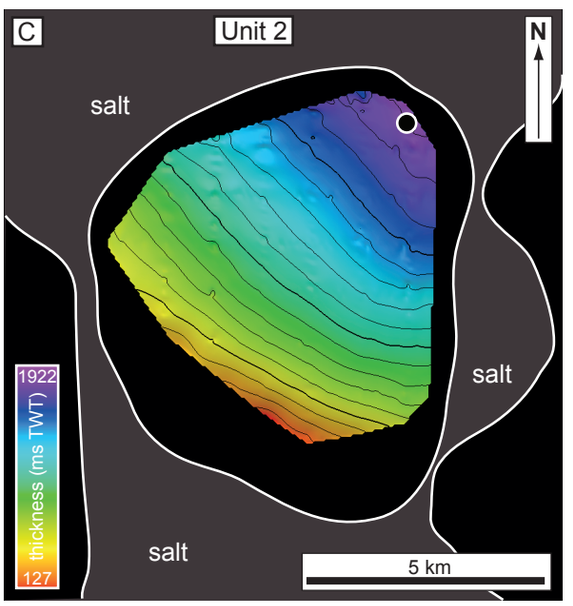
C
Unit 2
N
salt
1922
thickness (ms TWT)
127
5 km

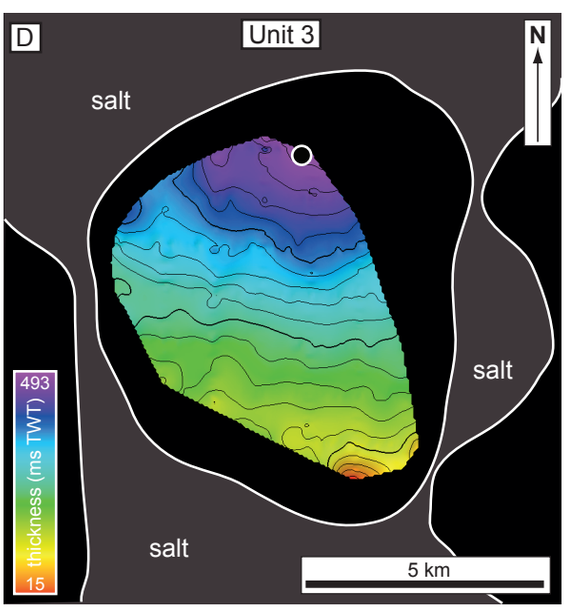
D
Unit 3
N
salt
493
thickness (ms TWT)
15
5 km

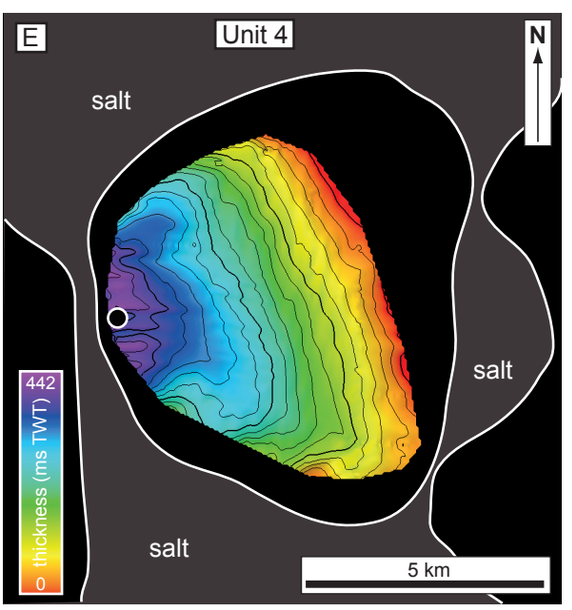
E
Unit 4
N
salt
442
thickness (ms TWT)
0
5 km

Fig. 9

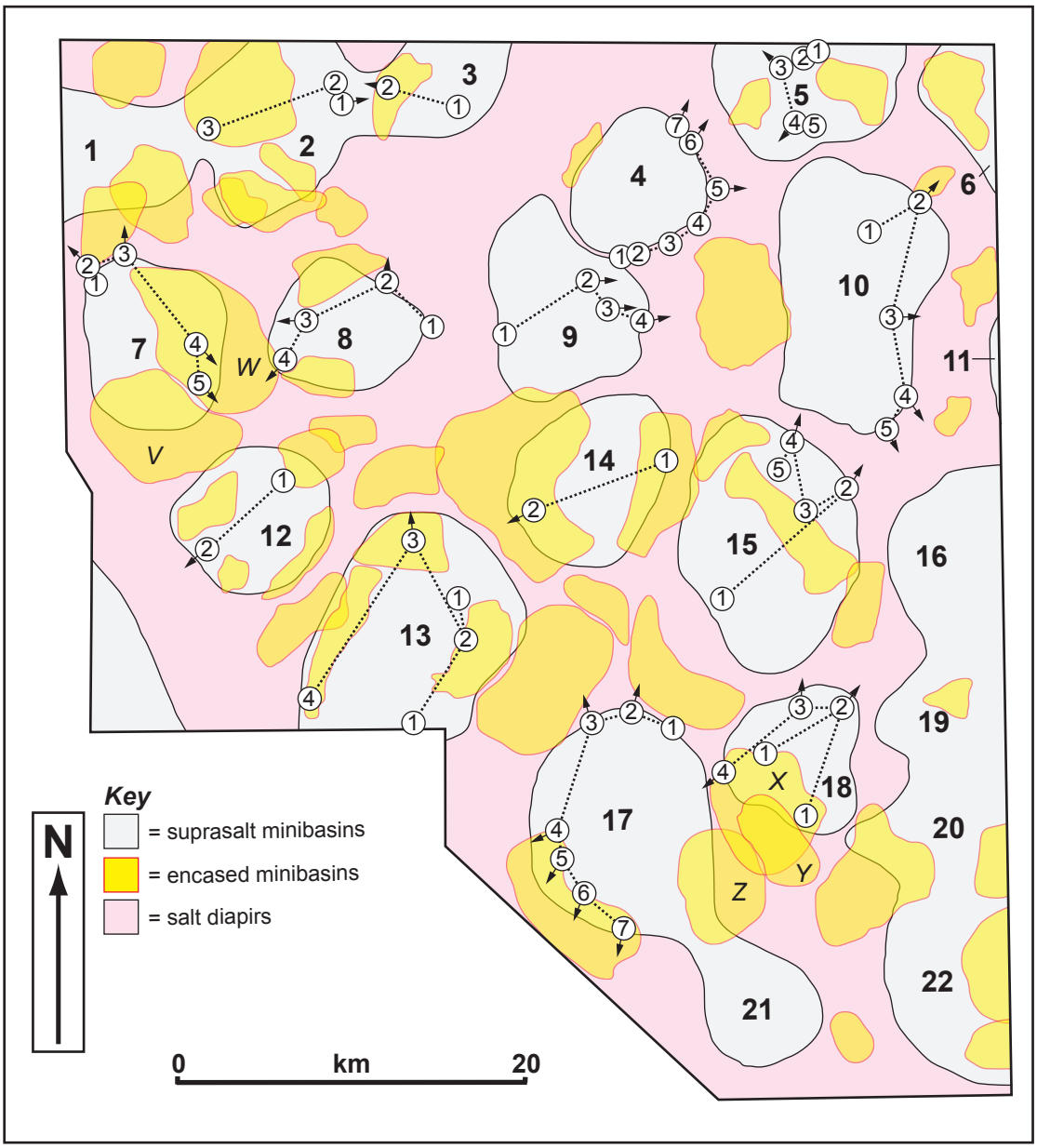
1
2
3
4
5
6
7
8
9
10
11
12
13
14
15
16
17
18
19
20
21
22
V
W
X
Y
Z
Key
= suprasalt minibasins
= encased minibasins
= salt diapirs
N
0
km
20

Fig. 10

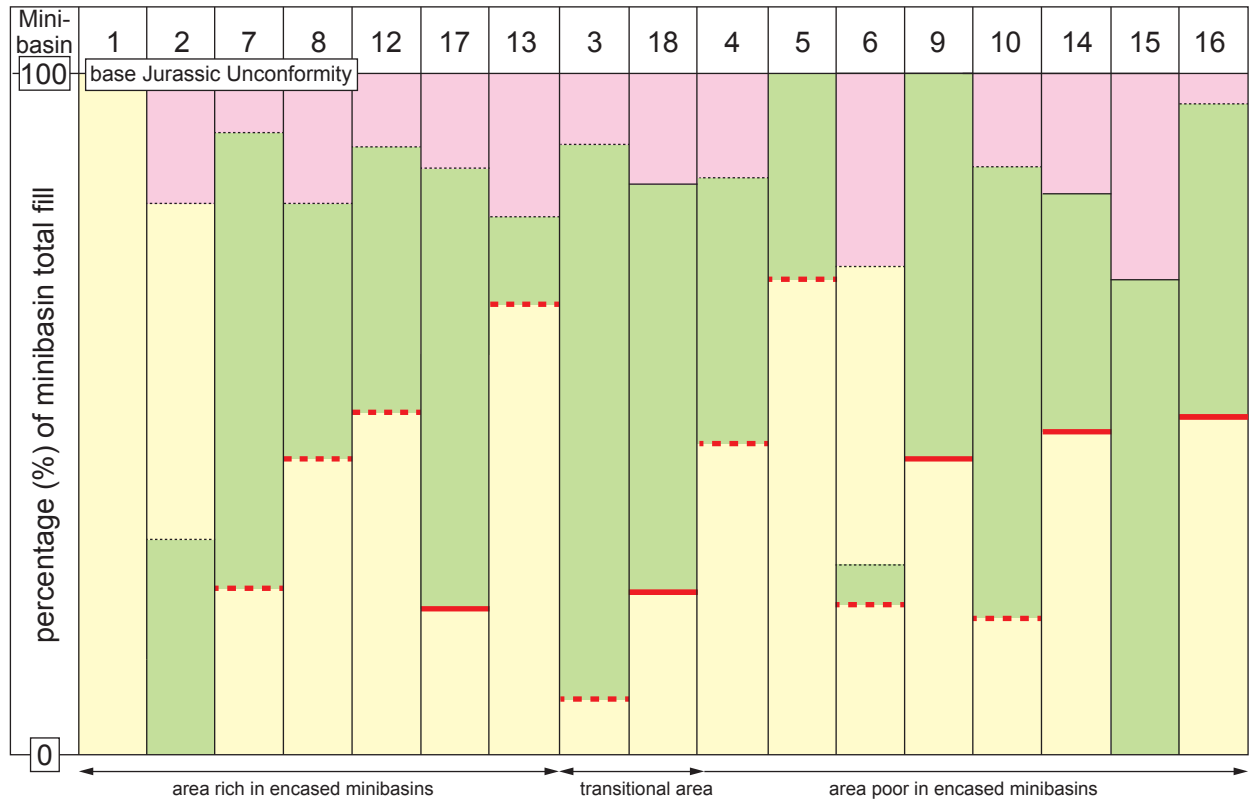

Key

= layers

= wedges

= bowls

= transitional boundary from bowl- to wedge-shaped seismic sequence

= abrupt boundary from bowl- to wedge-shaped seismic sequence

= transitional boundary from wedge- to layer-/wedge- to bowl-shaped seismic sequence

= abrupt boundary from wedge- to layer-shaped seismic sequence

Fig. 11

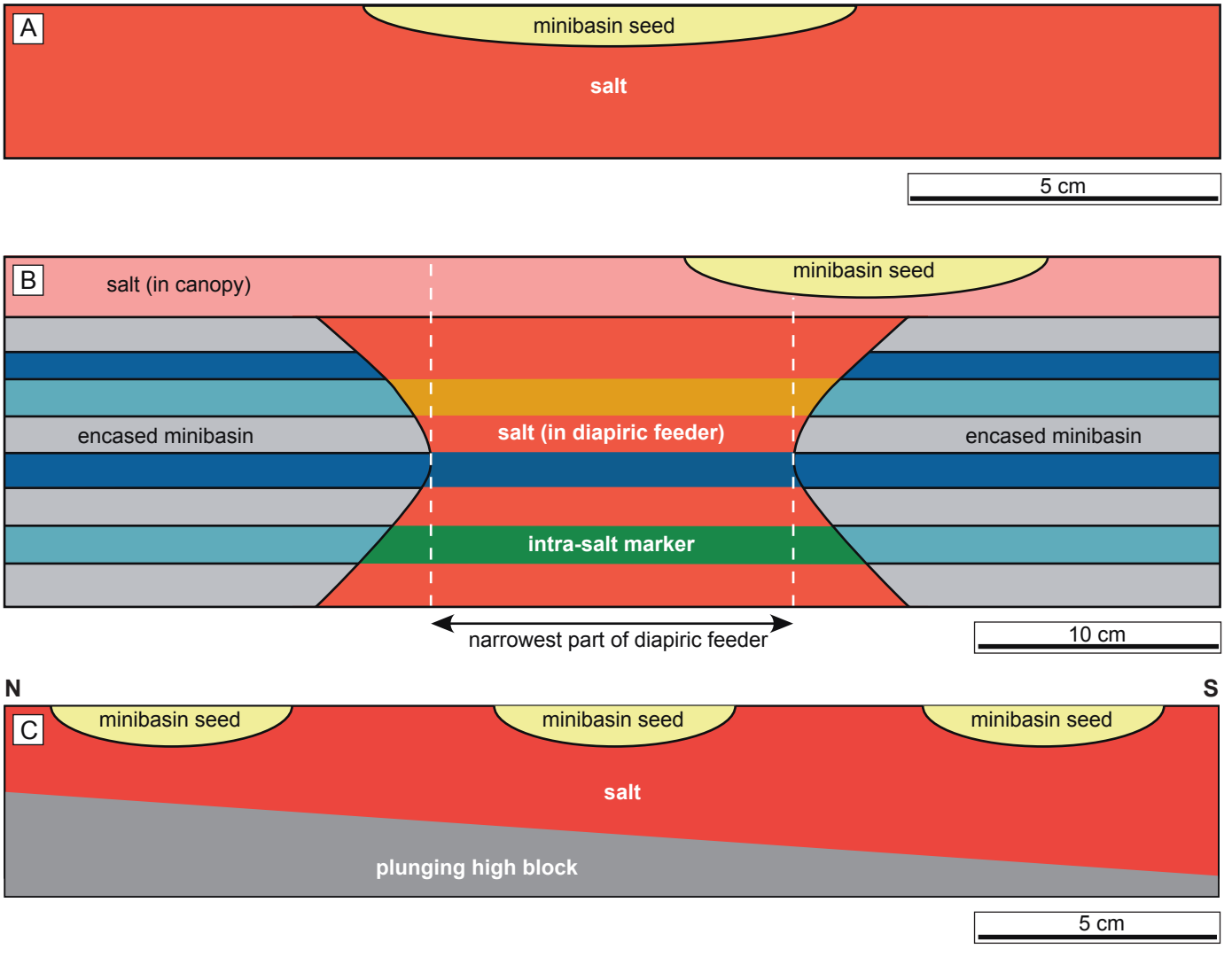
A
minibasin seed
salt
5 cm
B
salt (in canopy)
minibasin seed
encased minibasin
salt (in diapiric feeder)
encased minibasin
intra-salt marker
narrowest part of diapiric feeder
10 cm
N
S
C
minibasin seed
minibasin seed
minibasin seed
salt
plunging high block
5 cm

Fig. 12

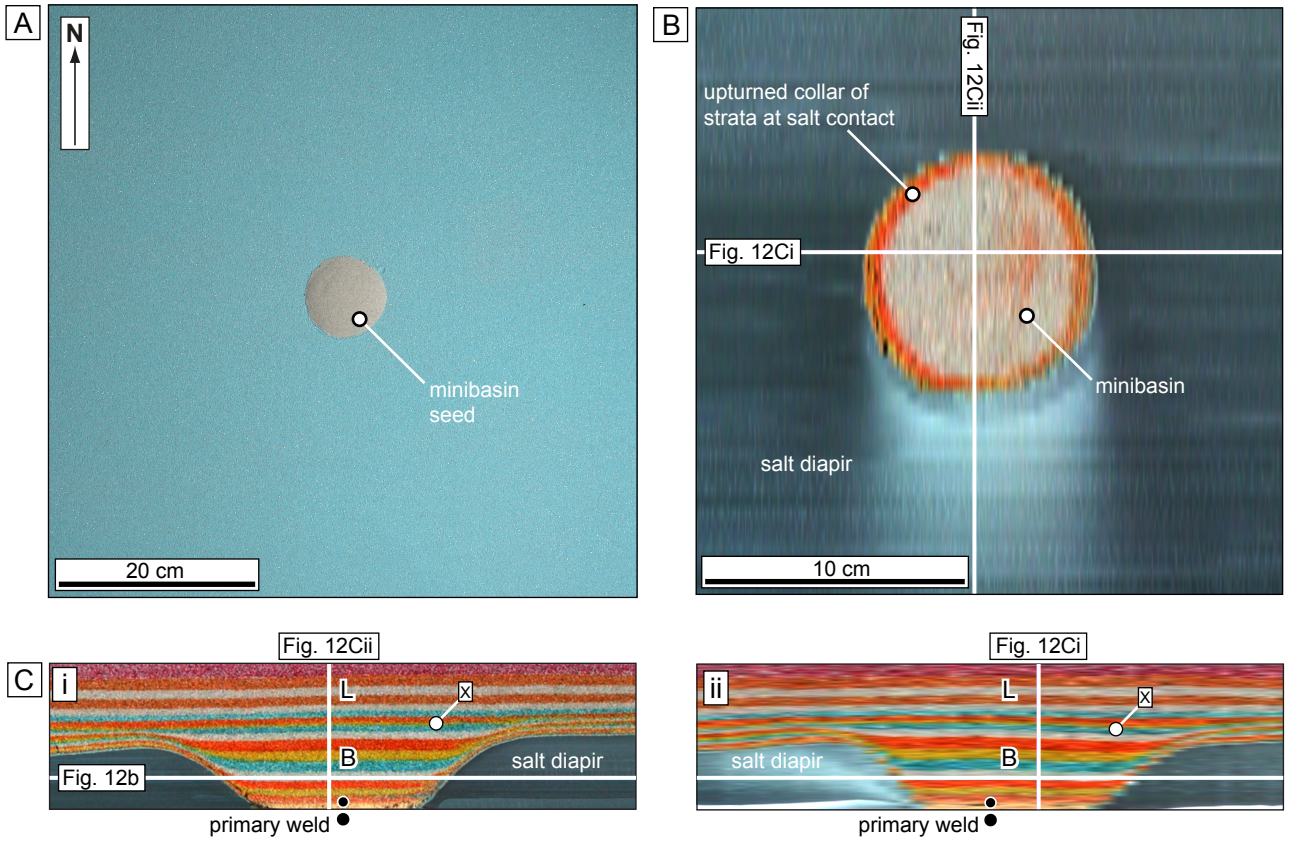
A
N
minibasin
seed
20 cm
B
Fig. 12Cii
upturned collar of
strata at salt contact
Fig. 12Ci
minibasin
salt diapir
10 cm
C
i
Fig. 12Cii
L
X
B
salt diapir
Fig. 12b
primary weld
ii
Fig. 12Ci
L
X
salt diapir
B
primary weld

Fig. 13

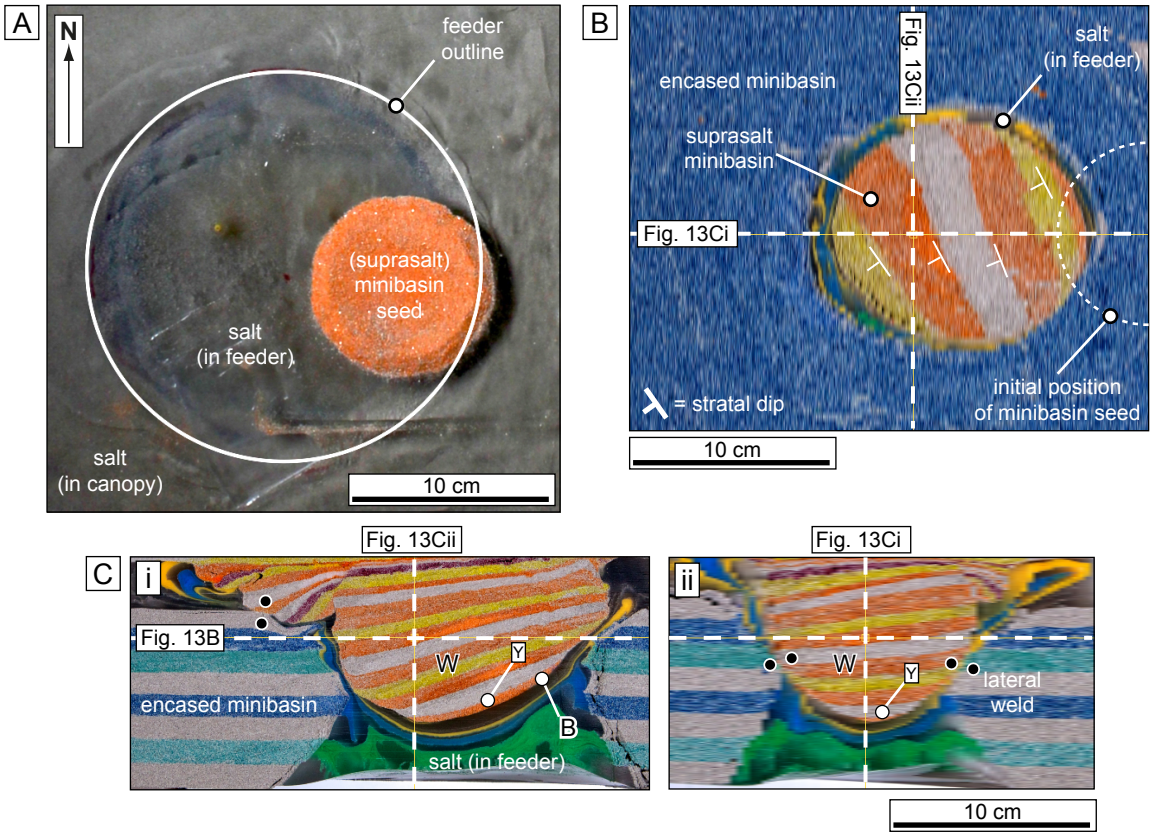
A
N
feeder
outline
(suprasalt)
minibasin
seed
salt
(in feeder)
salt
(in canopy)
10 cm
B
Fig. 13Cii
encased minibasin
salt
(in feeder)
suprasalt
minibasin
Fig. 13Ci
= stratal dip
initial position
of minibasin seed
10 cm
C
Fig. 13Cii
Fig. 13Ci
i
ii
Fig. 13B
W
Y
B
encased minibasin
salt (in feeder)
W
Y
lateral
weld
10 cm

Fig. 14

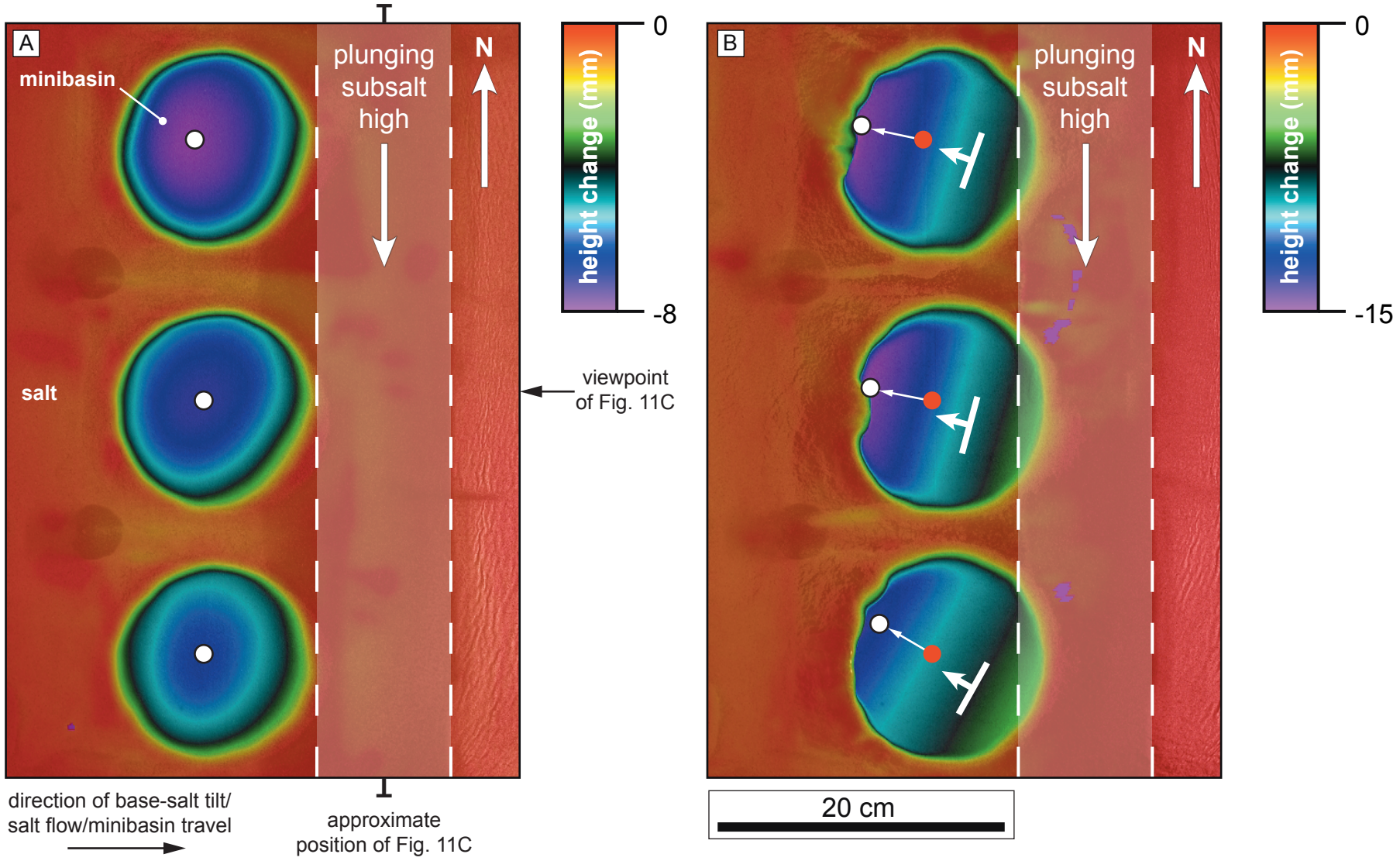
A
minibasin
salt
plunging
subsalt
high
N
height change (mm)
0
-8
viewpoint
of Fig. 11C
direction of base-salt tilt/
salt flow/minibasin travel
approximate
position of Fig. 11C
B
plunging
subsalt
high
N
height change (mm)
0
-15
20 cm

Fig. 15

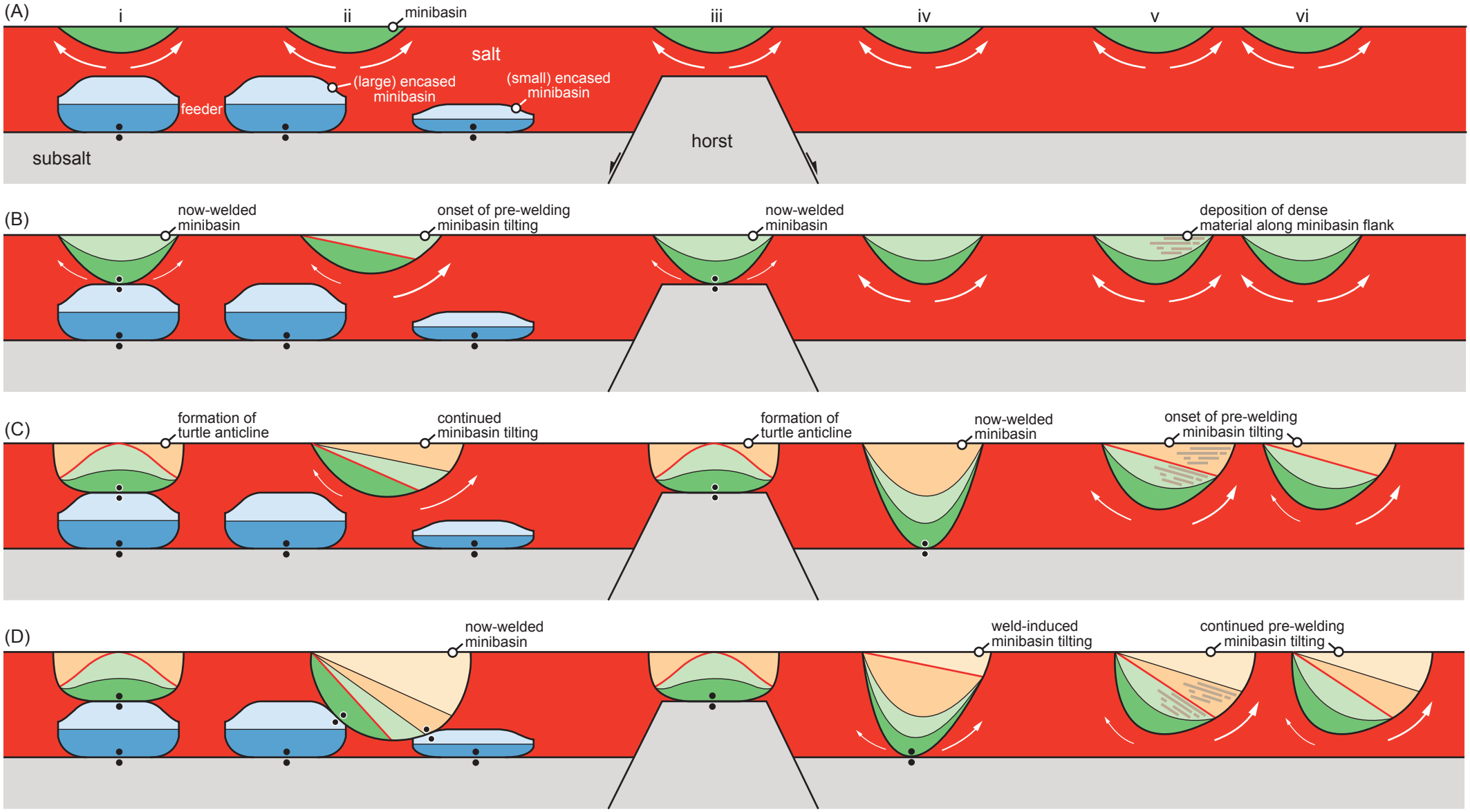
(A)
i
ii
minibasin
iii
iv
v
vi
salt
(large) encased minibasin
(small) encased minibasin
feeder
horst
subsalt
(B)
now-welded minibasin
onset of pre-welding minibasin tilting
now-welded minibasin
deposition of dense material along minibasin flank
(C)
formation of turtle anticline
continued minibasin tilting
formation of turtle anticline
now-welded minibasin
onset of pre-welding minibasin tilting
(D)
now-welded minibasin
weld-induced minibasin tilting
continued pre-welding minibasin tilting
Key
= stratigraphic surface defining onset of minibasin tilting/asymmetric subsidence
= intra-minibasin stratigraphic surface
= pre-existing weld
= newly formed weld
= salt flow (arrow size indicates vigour of flow)